

Dynamics of Monatomic Liquids

Eric D. Chisolm and Duane C. Wallace

T-1, Mail Stop B221
Los Alamos National Laboratory
Los Alamos, NM 87545

November 21, 2018

Abstract

We present a theory of the dynamics of monatomic liquids built on two basic ideas: (1) The potential surface of the liquid contains three classes of intersecting nearly-harmonic valleys, one of which (the “random” class) vastly outnumbers the others and all whose members have the same depth and normal mode spectrum; and (2) the motion of particles in the liquid can be decomposed into oscillations in a single many-body valley, and nearly instantaneous inter-valley transitions called *transits*. We review the thermodynamic data which led to the theory, and we discuss the results of molecular dynamics (MD) simulations of sodium and Lennard-Jones argon which support the theory in more detail. Then we apply the theory to problems in equilibrium and nonequilibrium statistical mechanics, and we compare the results to experimental data and MD simulations. We also discuss our work in comparison with the QNM and INM research programs and suggest directions for future research.

1 Introduction

Despite a long history of physical studies of the liquid state, no single theory of liquid dynamics has achieved the nearly universal acceptance of Boltzmann’s theory of gases or Born’s theory of lattice dynamics of crystals. This shows the extraordinary theoretical challenge that liquids pose; they enjoy

none of the properties that make either crystals or gases relatively tractable. A great deal of effort has been devoted to understanding liquids as hard-sphere systems, which do model the core repulsion present in real liquids, but omit the important potential energy effects. A more realistic view was given by Frenkel [1, 2], who noted that when a typical crystal melts neither its specific heat, cohesive properties, nor volume changes greatly, while its diffusion coefficient increases dramatically; he concluded from this that the basic motion of particles in a liquid consists of small oscillations about a set of equilibria, as in a solid, but that these equilibria are neither symmetrically arranged in space nor unchanging in time. This highly suggestive picture of a liquid as something like an amorphous harmonic solid with equilibrium positions that occasionally move around, allowing for diffusion, has inspired many extensive programs of research.

For example, after Stillinger and Weber’s computer simulations [3, 4] revealed the existence in the liquid of mechanically stable arrangements of particles, called inherent structures, with a wide range of energies, several workers have developed the idea that the liquid moves in a “rugged potential energy landscape” with a wide distribution of structural potential energies separated by barriers having a wide distribution of heights [5, 6]. These ideas have influenced the development of both the quenched normal mode, or QNM [6, 7, 8] and instantaneous normal mode, or INM [9, 10, 11, 12, 13, 14, 15] schools of thought.

Here we will review another line of inquiry which has been pursued for the last five years or so [16, 17, 18, 19, 20, 21, 22, 23, 24] and which differs from the others in that it begins by focusing on a restricted class of liquids (see below), and it proposes that they move in a significantly simpler potential landscape.

This work is concerned exclusively with monatomic liquids, meaning elemental liquids which do not exhibit molecular bonding. Monatomic liquids include all elemental liquid metals and the rare gas liquids, but not molecular liquids such as N_2 and O_2 , and not polyatomic systems such as alkali halides or water. Molecular liquids have translational, rotational, and internal vibrational degrees of freedom, while monatomic liquids have only translational motion, and the potential energy surface for monatomic liquids is presumably the simplest of all liquid potential landscapes. Our strategy is to develop a thorough understanding of this hopefully simplest case, and then to apply the insights gained there to more complex liquid systems.

In Section 2, we describe the thermodynamic data which led us to a spe-

cific picture of liquid dynamics, and we describe the picture itself in some detail. As will be clear, the thermodynamic data are consistent with the picture, but they do not lead to it uniquely; thus additional support is called for. In Section 3 we review the results of molecular dynamics (MD) studies of two particular liquids, sodium and Lennard-Jones argon, which support many of our claims in far more detail. Then we apply the picture in Sections 4 and 5 to problems in equilibrium and nonequilibrium statistical mechanics, and we compare the results to experimental data and MD simulations. In Section 6, we briefly review the picture, compare it with other research programs, consider the current status of its verification, discuss further problems to which it may be applied, and describe the role we believe it fills in the continuing effort to develop a comprehensive theory of the dynamics of liquids.

2 The picture

2.1 Thermodynamic data

Initial support for our picture comes from an analysis of two types of thermodynamic data: The constant-volume specific heat C_V at the melting point of various monatomic liquids, and the entropy of melting of these elements.

2.1.1 Specific heat

The experimentally determined specific heats at constant pressure C_P for the elements have been compiled by Hultgren et al. [25] and Chase et al. [26] for both crystal and liquid phases at the melting point; these can be corrected in the standard way to determine C_V . C_V is composed of the contributions C_I from the motion of the ions and C_E from the excitation of the valence electrons,

$$C_V = C_I + C_E, \quad (1)$$

and for the nearly-free-electron elements the electronic contribution is given accurately by

$$C_E = \frac{1}{3} \pi^2 N k_B^2 T n(\epsilon_F), \quad (2)$$

where $n(\epsilon_F)$ is the electron density of states per atom at the Fermi energy ϵ_F . Thus Wallace [16] chose to study the nearly-free-electron elements, for

which C_I can be accurately determined. He took $n(\epsilon_F)$ from band structure calculations when possible [27, 28] and from free-electron theory otherwise; then he subtracted out the electronic contribution to C_V , and the resulting ionic contributions for both the crystal and liquid phases are shown in Figure 1, which is adapted from Figure 1 of [17]. The quantities predicted by hard-sphere theory are shown for comparison. Notice that all elements cluster around $C_I = 3Nk_B$ in both phases. (The exception is argon at 1 bar, which is known to be rather gaslike, but at pressures approaching 1 kbar its behavior more closely resembles that of the other liquids; thus, we will henceforth consider only compressed argon.) It is known that any of the crystals may be modeled very accurately as a set of $3N$ harmonic oscillators, thus accounting for their specific heats; this is the starting point of lattice dynamics. That the liquids at melt have nearly the same values for C_I suggests that they too behave as harmonic oscillators. The departures from harmonicity for both phases lie outside the experimental errors; anharmonic effects on the C_I of liquids will be discussed in Sections 4 and 6.

2.1.2 Entropy of melting

A study of the entropy of melting at constant density (but not constant pressure) of a large number of monatomic liquids led Wallace [29, 30] to suggest that the elements can be separated into two classes: the “normal melting elements,” for which $\Delta S = (0.80 \pm 0.10)Nk_B$, and the “anomalous melting elements,” for all of which ΔS lies far above the range of the normal melters. The entropy of melting results are shown in Table 1, which is adapted from Table III of [30]. The first column is the set of normal melters used to calculate the number given above; the second is a set of transition metals, which reasonably may be considered normal melters (but not anomalous melters) given the larger errors in their ΔS data. The six anomalous melters are in the final column. The electronic structures of the normal melters do not change greatly upon melting, while for the anomalous melters the structure change is noticeable (semimetal crystal to metal liquid, semiconductor crystal to metal liquid, etc.), and this change is presumably responsible for the excess contribution to ΔS . Considering only the normal melting elements for a moment, this change in entropy upon melting is consistent with a scenario in which the system, which had previously been confined to a single crystalline potential valley, upon melting suddenly finds itself able to move over a space of approximately w^N valleys where $\ln w = 0.8$; the entropy increase is due

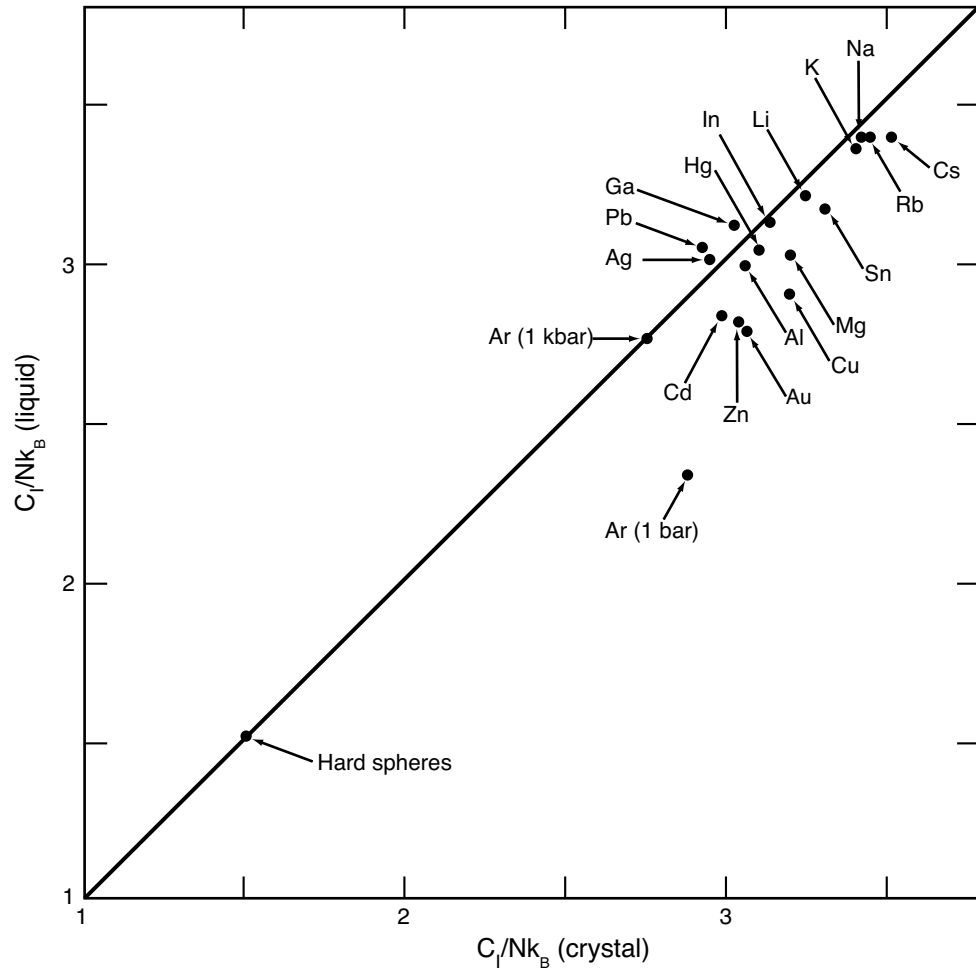


Figure 1: Ion-motional specific heat for 18 elements in both liquid and crystal phases at melt. Adapted from [17].

Element	$\Delta S/Nk_B$	Element	$\Delta S/Nk_B$	Element	$\Delta S/Nk_B$
Li	0.75	V	0.90	Sn	1.48
Na	0.73	Nb	0.97	Ga	2.37
K	0.73	Ta	1.1	Sb	2.68
Rb	0.73	Cr	(0.9)	Bi	2.62
Cs	0.73	Mo	(1.2)	Si	3.77
Ba	0.90	W	(1.1)	Ge	3.85
Fe	0.68	Pd	0.74		
Al	0.88	Pt	0.79		
Pb	0.68	Ti	0.70		
Cu	0.86	Zr	0.93		
Ag	0.73				
Au	0.64				
Ni	0.88				
Mg	0.96				
Zn	0.97				
Cd	0.93				
In	0.76				
Hg	0.90				

Table 1: Entropy of melting at constant density for 34 elements. The normal melting elements are in the first two columns, and the anomalous melting elements are in the third column. Data in parentheses are less reliable. Adapted from [30].

to the greater size of the available configuration space. (Strictly speaking, this is true only if certain other restrictions are satisfied; see Subsection 4.4 for a more extensive discussion.) We hypothesize that this change occurs for all melters, normal and anomalous, and that additional factors deriving from the change in the electronic structure account for the difference between the two cases. We return to the anomalous melters in Section 6.

2.2 Details of the picture

The data considered so far suggest that particles in a liquid move in a potential landscape dominated by harmonic valleys. We have refined this observation into a more precise picture of both the motion of the particles and the nature of the potential energy surface in which they move.

2.2.1 The motion

We hypothesize that the motion of the system may be decomposed into two distinct types: Oscillation in a single nearly harmonic many-body valley, and nearly instantaneous transitions between valleys which we call *transits*. That the valleys are nearly harmonic, and that the transits are nearly instantaneous, are both suggested by the C_I data, since C_I in all cases is quite close to the value expected for equilibrium motion in a single harmonic valley. In fact, any significant departure from this behavior should show itself clearly in the C_I data, so we believe that this part of the picture is very solidly supported by experiment. (Higher order corrections, to account for the small deviations of C_I from precisely $3Nk_B$, are considered in Subsection 4.3 and discussed in more detail in Section 6.) We also expect transits to involve only a few particles in the system at a time, because transits perform a function in liquids analogous to that performed by collisions in a Boltzmann gas: They drive the system irreversibly toward equilibrium, and once there, they maintain equilibrium by constantly opposing fluctuations. Mechanisms of equilibration operate on a local level, since any small region can equilibrate independently of the rest (except for equilibria involving macroscopic coherent quantum states, not considered here), so we expect transits to operate locally. Unlike gases, though, in which collisions almost always involve only two particles at a time, in liquids slightly larger groups of particles can undergo cooperative motion, since they are sufficiently close together that interparticle potentials are always significant, so a single transit could involve

as many as tens of particles.

2.2.2 Types of potential valleys

If the valleys in the many-body potential surface are nearly harmonic, then each is characterized by its structure potential Φ_0 , defined to be the value of the system's potential energy at the bottom of the valley, and its density of normal mode frequencies $g(\omega)$. We also hypothesize that the valleys may be divided into three classes: crystalline, symmetric, and random.

(1) A *crystalline* valley is occupied when the system is in one of its crystalline phases. These valleys are very few in number, and since the crystalline phases are the most stable at low temperatures, they also have the lowest value for their structure potential Φ_0 . Due to their very small number, the crystalline valleys make a negligible contribution to the statistical mechanics of the liquid.

(2) The *symmetric* valleys correspond to more disordered configurations that still retain some remnant of crystalline symmetry. This group includes a large variety of polycrystalline and microcrystalline types, as well as the states of carbon realized experimentally by McKenzie, Muller, and Pailthorpe [31] which differ from the perfect diamond by irregularly distorted bond lengths and angles. These valleys are more shallow than the crystalline ones, and their structure potentials Φ_0 are expected to cover a wide range of values due to their large variety of symmetry properties. Also because of their widely varying symmetries, we expect the normal mode spectrum $g(\omega)$ to vary substantially from valley to valley.

(3) Finally, the *random* valleys are occupied when the system retains no remnant crystalline symmetries. Since their configurations suffer no symmetry restrictions, these valleys should greatly outnumber both the crystalline and symmetric valleys; in fact, we hypothesize that almost all of the w^N valleys available to the liquid are random, so the random valleys dominate the statistical mechanics of the liquid. Further, since the random valleys have no symmetry properties that allow them to be distinguished from one another, we expect that in the large- N limit all random valleys should have the same structure potential Φ_0 and normal mode spectrum $g(\omega)$, in stark contrast to both the crystalline and symmetric valleys. (In the examples we have studied, Φ_0 for the random valleys always lies above the Φ_0 values for all of the symmetric valleys, but we see no reason for this to be true over the entire potential surface.)

The hypothesis that the vast majority of valleys available to a monatomic liquid have the same depth and vibrational spectrum is a distinctive part of our approach, and it has extraordinary consequences for the statistical mechanics of the liquid; however, it is clear that the data considered to this point lend that idea scant support. Thus further studies were conducted to test the validity of this picture for specific monatomic liquids; these studies are discussed next.

3 Verifying the picture

Our picture of monatomic liquids consists of two sets of hypotheses: Those concerning the motion of the system, particularly that transits occur rapidly and involve only a few particles; and those concerning the potential energy surface and the classification of valleys into three types. We consider tests of each set of hypotheses in turn.

3.1 Transits

To investigate the properties of transits, we conducted computer simulations of two liquids: sodium and Lennard-Jones argon.

3.1.1 Sodium

Our simulation of an N -atom sodium system is described in detail in [19]. The particles interact through a potential of the general form [32, 33]

$$\Phi(\{\mathbf{r}_K\}) = \Omega(V) + \frac{1}{2} \sum_{K,L} \phi(|\mathbf{r}_K - \mathbf{r}_L|; V), \quad (3)$$

where the strongly negative $\Omega(V)$ is responsible for metallic binding and the effective ion-ion potential $\phi(r; V)$ is given by pseudopotential theory [34]. This pair potential is shown in Figure 1 of [19]; it is multiplied by a damping factor to remove long-range Friedel oscillations, and this is the only significant effect of the factor on the potential. After being calibrated to the bulk properties of crystalline sodium at 0 K, the full potential in Equation (3) has been shown to reproduce with remarkable accuracy several known properties of metallic sodium, such as the phonon frequency spectrum and the melting temperature as a function of pressure. In our simulations, the volume per

atom $V_A = V/N$ was fixed at $278 a_0^3$, where a_0 is the Bohr radius; this is the density of liquid sodium at melt when the pressure is 1 bar and the melting temperature is 371 K. Since V is held constant in our MD calculations, we chose to set $\Omega(V)$ to zero. The rms vibrational frequency of a typical many-body valley in this potential is $1.56 \times 10^{13} \text{ s}^{-1}$. (See Subsection 3.2 for more on the structure of potential valleys in sodium.) Calculations were performed using the Verlet algorithm [35] for a system in a cubical box with periodic boundary conditions; the natural time scale of the system is $t^* = \sqrt{2Ma_0^3/e^2}$, where M is the atomic mass of sodium, or $t^* = 7.00 \times 10^{-15} \text{ s}$. (The mean vibrational period in a typical potential valley is $\tau = 57.45 t^*$.) The two parameters which varied between runs were the number of particles N and the MD time step δt , which was always taken to be some fraction of t^* . We will refer frequently to MD studies of sodium through the rest of the paper, and each time we will indicate the values of each of these parameters.

We searched for transits in an $N = 500$ system where the time step was set to $\delta t = 0.2 t^*$. We cooled the system to a sufficiently low temperature that once it had equilibrated it remained in a single valley, as could be verified from its mean-squared displacement. We then raised the temperature by very small increments, each time allowing the system to equilibrate again, until transits began to occur at $T = 30 \text{ K}$. (The details of our method of searching for transits may be found in [24].) The x, y , and z coordinates of a particle in a typical transit are shown in Figure 2. Our general observations in sodium are as follows [24]: Every particle in the system either oscillated for the entire run around a single location, or it executed a transit of the general type seen in Figure 2, where the particle oscillated in a single region of space for some time, abruptly moved to a new region, and continued to oscillate in the new region. Typically small groups of particles transited simultaneously, and many more particles would execute smaller shifts in their equilibrium positions during a small window in time around the transit. Further, it was not uncommon for a single particle to participate in two or three transits, well separated from one another in time. The average shift in the equilibrium position of a particle involved in a transit was $1.75 a_0$ (about one quarter of the nearest neighbor distance of $7a_0$); the average duration in time of any transit was τ , and this includes the time taken by precursors and postcursors to some of the transits (described below in the discussion of argon). Thus our general picture of transits as abrupt transitions between equilibrium positions of a small group of particles is supported in this system.

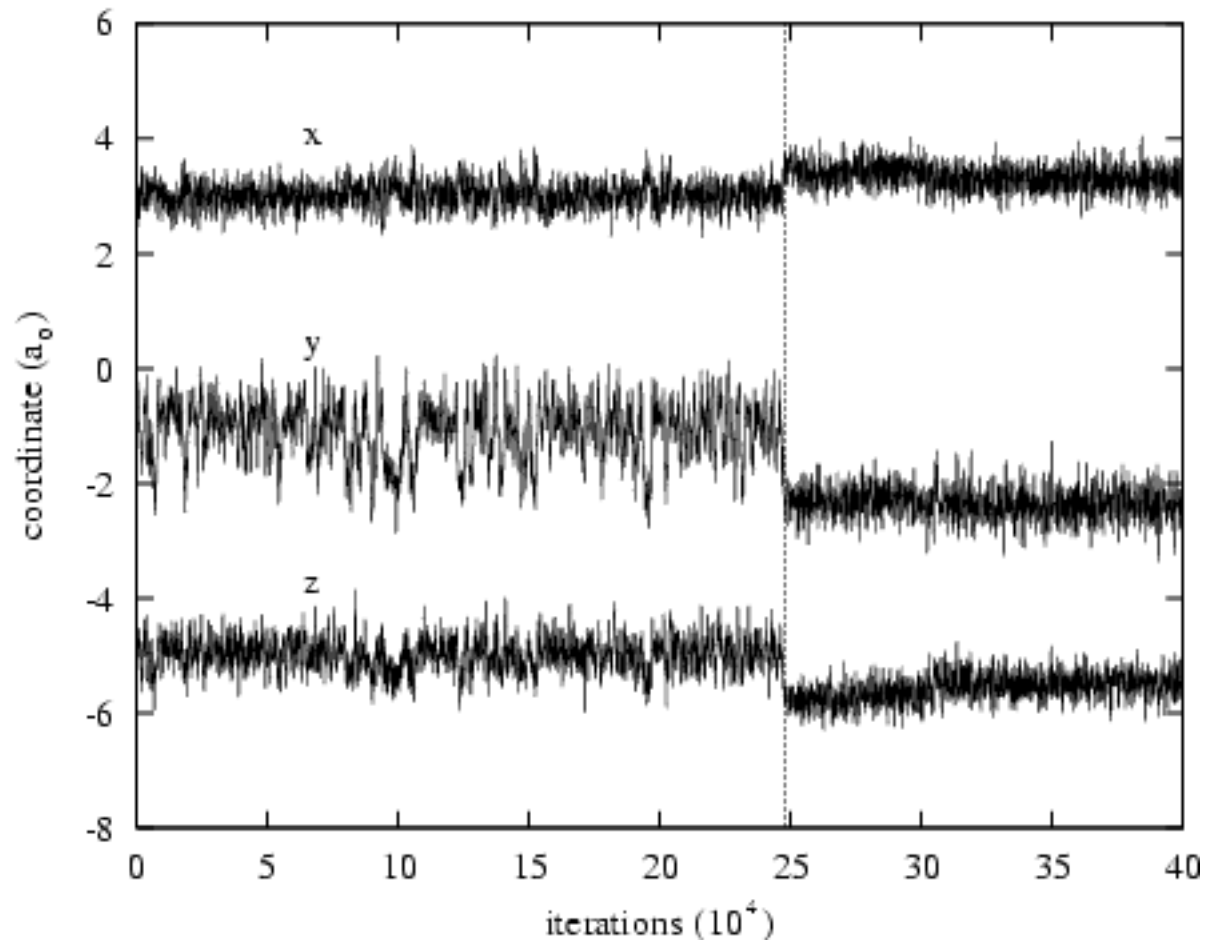


Figure 2: The coordinates of one particle in an 11-particle transit in sodium at 30 K. Adapted from [24].

3.1.2 Lennard-Jones argon

Our simulation of argon consists of N particles interacting through a Lennard-Jones pair potential

$$\phi(r) = 4\epsilon \left[\left(\frac{\sigma}{r} \right)^{12} - \left(\frac{\sigma}{r} \right)^6 \right] \quad (4)$$

where $\epsilon = 1.65 \times 10^{-21}$ J (with equivalent temperature 119.8 K) and $\sigma = 3.405$ Å. The density was set to 0.9522 particles/ σ^3 , or 1.600 g/cm³. (The density of liquid argon at melt at 1 bar is 1.414 g/cm³.) The rms vibrational frequency of a typical many-body valley in this potential is 6.88×10^{12} s⁻¹. (See Subsection 3.2 for more on the structure of potential valleys in argon.) Calculations were performed again using the Verlet algorithm for a box with periodic boundary conditions; the natural time scale of this system is $t^* = \sqrt{M\sigma^2/\epsilon}$, where M is the atomic mass of sodium, or $t^* = 2.16 \times 10^{-12}$ s. (The mean vibrational period in a typical potential valley is $\tau = 0.424 t^*$.) The time step in all MD calculations was $\delta t = 0.001 t^*$; the only parameter varied between argon runs was N .

We searched for transits in an $N = 500$ system using the same technique that was used for sodium; we found transits at 17.1 K. The z coordinates of three particles involved in an 8-particle transit are shown in Figure 3. The horizontal dotted lines indicate the equilibrium positions of the particles before and after the transit; the vertical line indicates the transit time. All of the general observations made above about transits in sodium also hold here [24]: The type of motion seen in Figure 3 is typical, usually small groups of particles transited simultaneously, and individual particles sometimes participated in multiple distinct transits. The average shift in the equilibrium position of a particle involved in a transit was 0.44σ (about four tenths of the nearest neighbor distance of 1.095σ); the average duration in time of any transit was again τ , and again this includes the time taken by precursors and postcursors to some of the transits. By a precursor or postcursor, we mean a slow drift by a single particle into a new equilibrium position either before or after a multiple-particle transit; a typical precursor is shown in Figure 4, part of the record of a 3-particle transit that occurred roughly 13τ after the transit shown in Figure 3. Every drift of the type seen in Figure 4 that we found occurred in connection with a transit, so we believe that precursors and postcursors are part of the transit process. They are the primary reason that the duration of a typical transit in either system is as high as τ ;

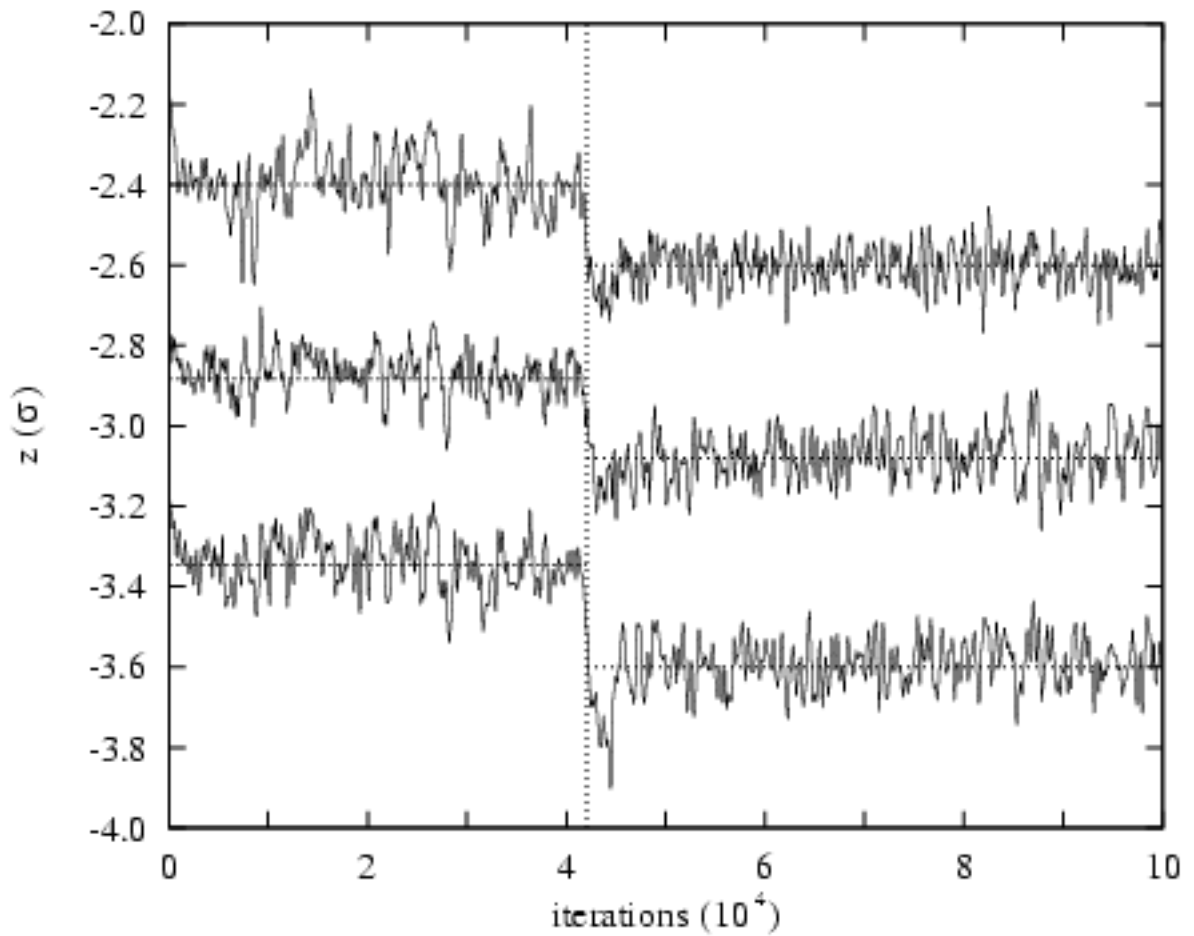


Figure 3: The z coordinates of three particles from an 8-particle transit in Lennard-Jones argon at 17.1 K. Adapted from [24].

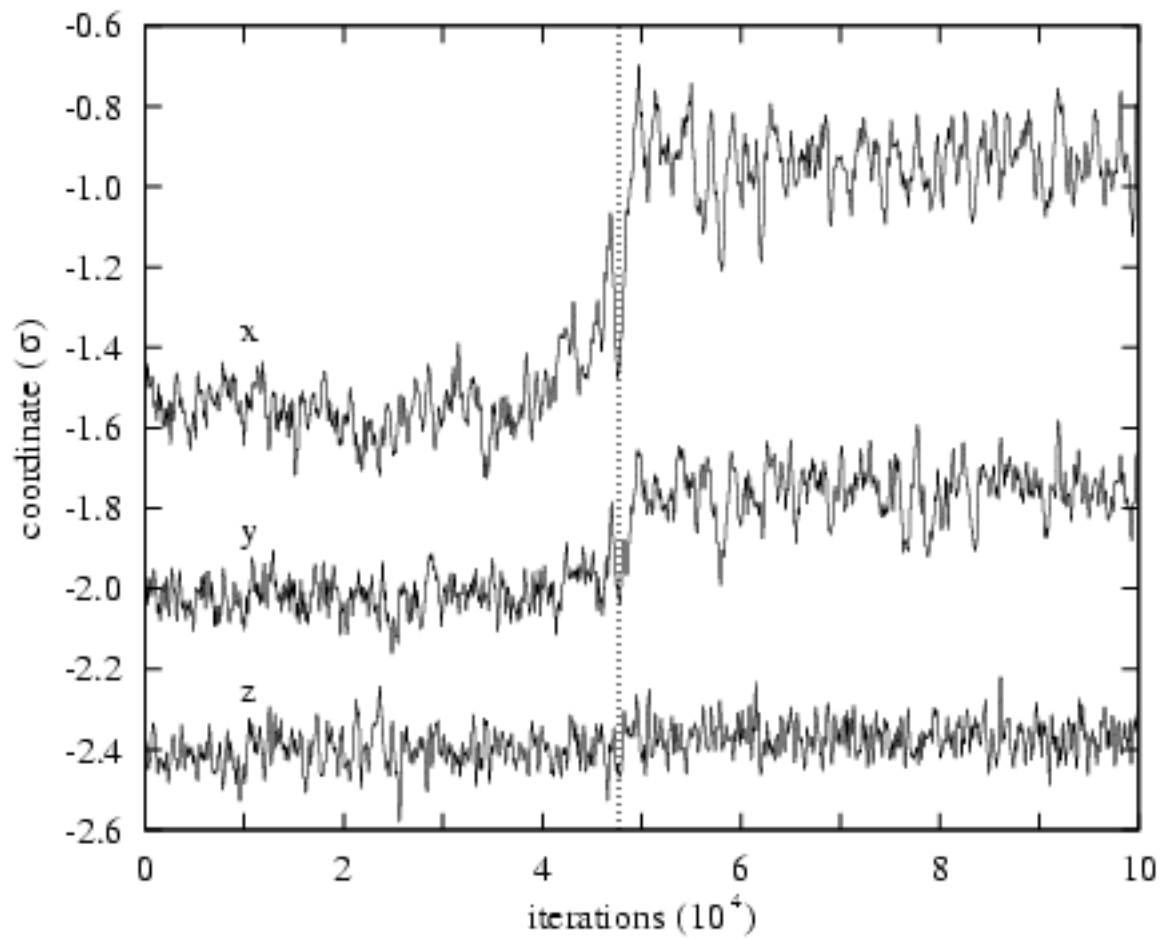


Figure 4: The coordinates of one of three particles involved in a transit in Lennard-Jones argon at 17.1 K. Note the precursor, which is particularly visible in the x coordinate. Adapted from [24].

many transits are of essentially zero duration when one neglects these effects, and most transits exhibit no precursors or postcursors and so are genuinely nearly instantaneous. Thus we conclude that our basic picture of the motion of particles in a liquid as a combination of oscillations and transits is verified in these cases. The precursors and postcursors are still of some interest, however, and we will comment on them again in Section 6.

3.2 Structure of the many-body potential landscape

3.2.1 Sodium

Wallace and Clements [19, 20] conducted an exhaustive study of the many-body potential underlying the sodium simulations in order to test the validity of the three-fold classification of valleys proposed above. They generated a large number of supercooled equilibrium states of systems with $N = 500$, 1000, and 3000 and cataloged properties such as their energies and pair distribution functions. They made the following observations about the states:

(1) A graph of time-averaged potential energy per particle $\langle\Phi/N\rangle$ versus time-averaged kinetic energy per particle $\langle\mathcal{K}/N\rangle$ for the equilibrium states is shown in Figure 5. The melting temperature $T = 371$ K corresponds to $\langle\mathcal{K}/N\rangle = 3.53$ mRy, so all of the states in the figure are supercooled, as claimed. This figure also shows the curve occupied by the bcc crystal states and the path followed by a typical MD run used to generate the states: Several quenches keep the kinetic energy at zero while the system moves down the path of steepest descent on the potential energy surface, so its potential energy continues to decrease; and when the quenches end the system equilibrates under the condition that $\Phi + \mathcal{K}$ remains constant, so the system moves down the 45° line on the graph. Notice that the states separate cleanly into two distinct groups. Each group of states lies approximately along a line with unit slope, as predicted by the equipartition theorem if the states are moving in harmonic valleys, although the lower group shows considerable scatter and the slope of the upper line increases at higher temperatures. Thus we tentatively suggest that for each N the system is moving in a landscape of approximately harmonic valleys, but we also see significant anharmonic effects to which we will return later.

(2) The system almost always quenched into one of the states from the upper group first; if the temperature was between approximately 35 K and 200 K, it would remain in such a state for several thousand time steps (long

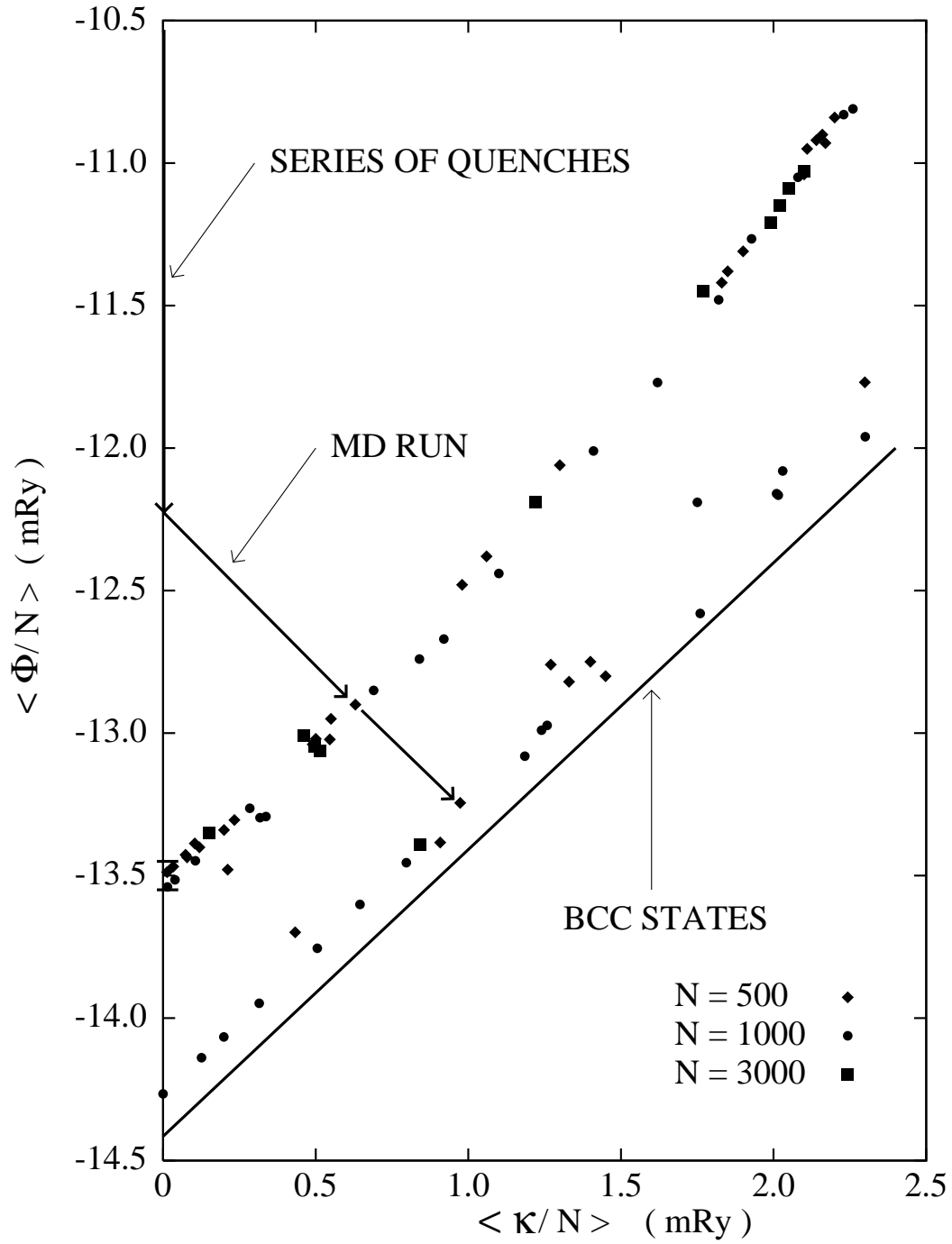


Figure 5: $\langle \Phi/N \rangle$ versus $\langle \mathcal{K}/N \rangle$ for several equilibrium states in sodium. From [19].

enough to compute equilibrium data) before settling spontaneously into one of the states in the lower group. It would remain in this state for as long as the MD run proceeded.

(3) The states in the upper group lie along the same curve as the equilibrium states of the liquid, while the states from the lower group appear to be bounded in energy by the limits of the graph.

(4) As T is increased, the graph of the pair distribution function $g(r)$ for the states from the upper group smoothly evolves into $g(r)$ for the liquid state, as shown in Figure 6.

(5) For a state from the lower group at temperatures above 100 K, $g(r)$ exhibits a split second peak, with the first subpeak lower than the second.

(6) By observing the mean-squared displacement of each state, defined by

$$d(t) = \frac{1}{6N} \sum_K [\mathbf{r}_K(t) - \mathbf{r}_K(0)]^2, \quad (5)$$

Wallace and Clements found that low-temperature states from both groups were confined to individual valleys of the potential surface. Let d be the time average of $d(t)$, or $d = \langle d(t) \rangle_t$. Then for a system in equilibrium in a single many-body harmonic valley,

$$d = \frac{3\hbar^2 T}{Mk_B \Theta_{-2}^2}, \quad (6)$$

where Θ_{-2} (defined below) is one of the principal moments of the valley's frequency distribution. (For a derivation, including some subtleties involving the omission of zero-frequency modes corresponding to center of mass motion, see [19].) Thus, if these states are confined in harmonic valleys, d should be a linear function of T . As we will note below, all of the valleys occupied by confined states in the upper group have the same frequency distribution, and thus the same Θ_{-2} ; Figure 7 shows d for several confined states in the upper group compared with Equation (6) using the common value of Θ_{-2} . The superb agreement further suggests that the valleys in which these states are trapped are in fact harmonic. Figure 13 of [19] shows that the same relation holds for several states from the lower group, all of which are confined to the same valley; however, Θ_{-2} is different for different valleys occupied by lower states (see below), so states from different valleys fit curves with different slopes.

Next, Wallace and Clements studied the actual many-body potential valleys occupied by the confined states, determining properties such as each

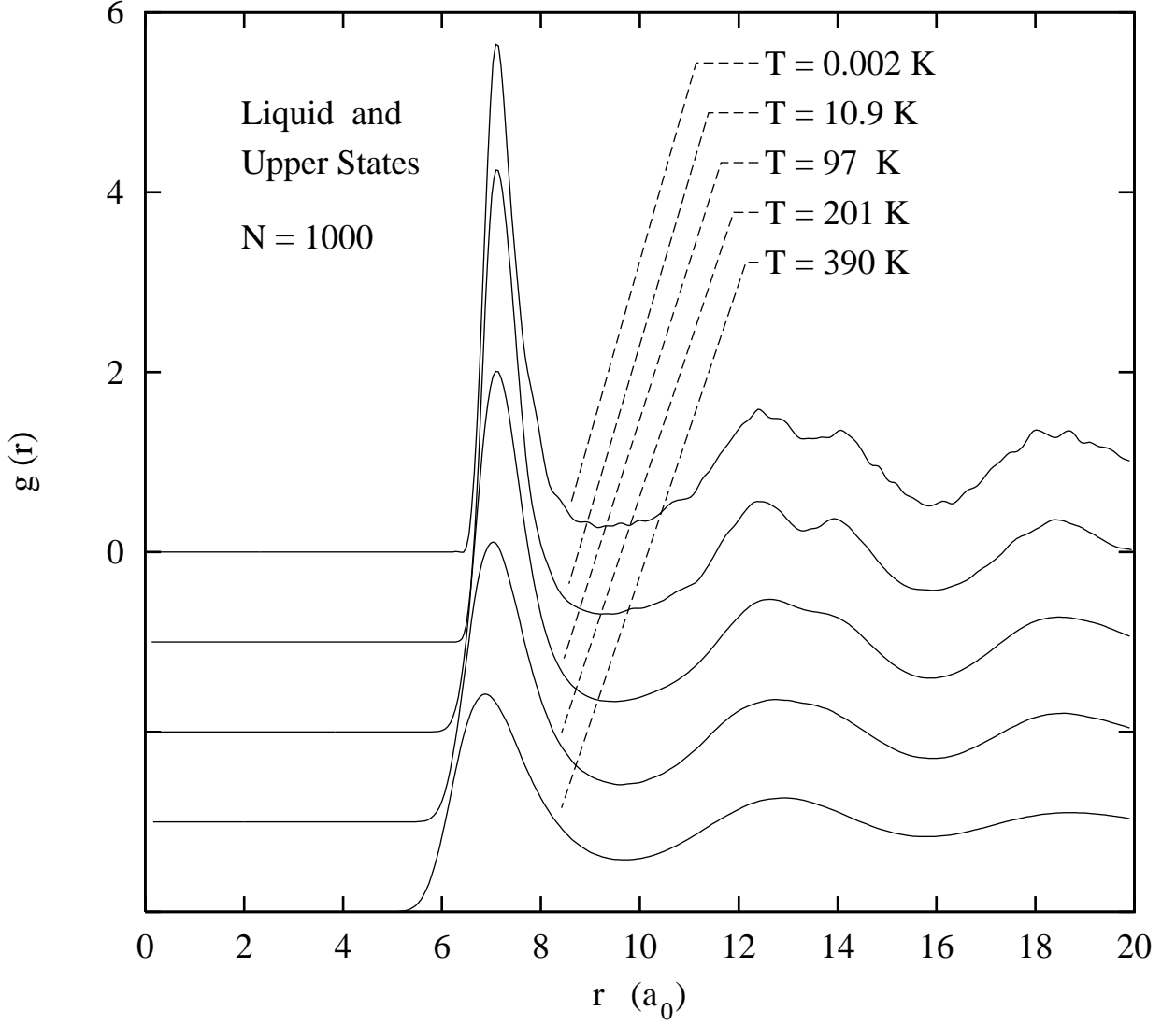


Figure 6: The pair distribution function for the liquid at 390 K and pair distribution functions for various states from the upper group at temperatures from 0.002 K to 201 K. Notice how the states continuously evolve into the liquid state with increasing temperature. Adapted from [20].

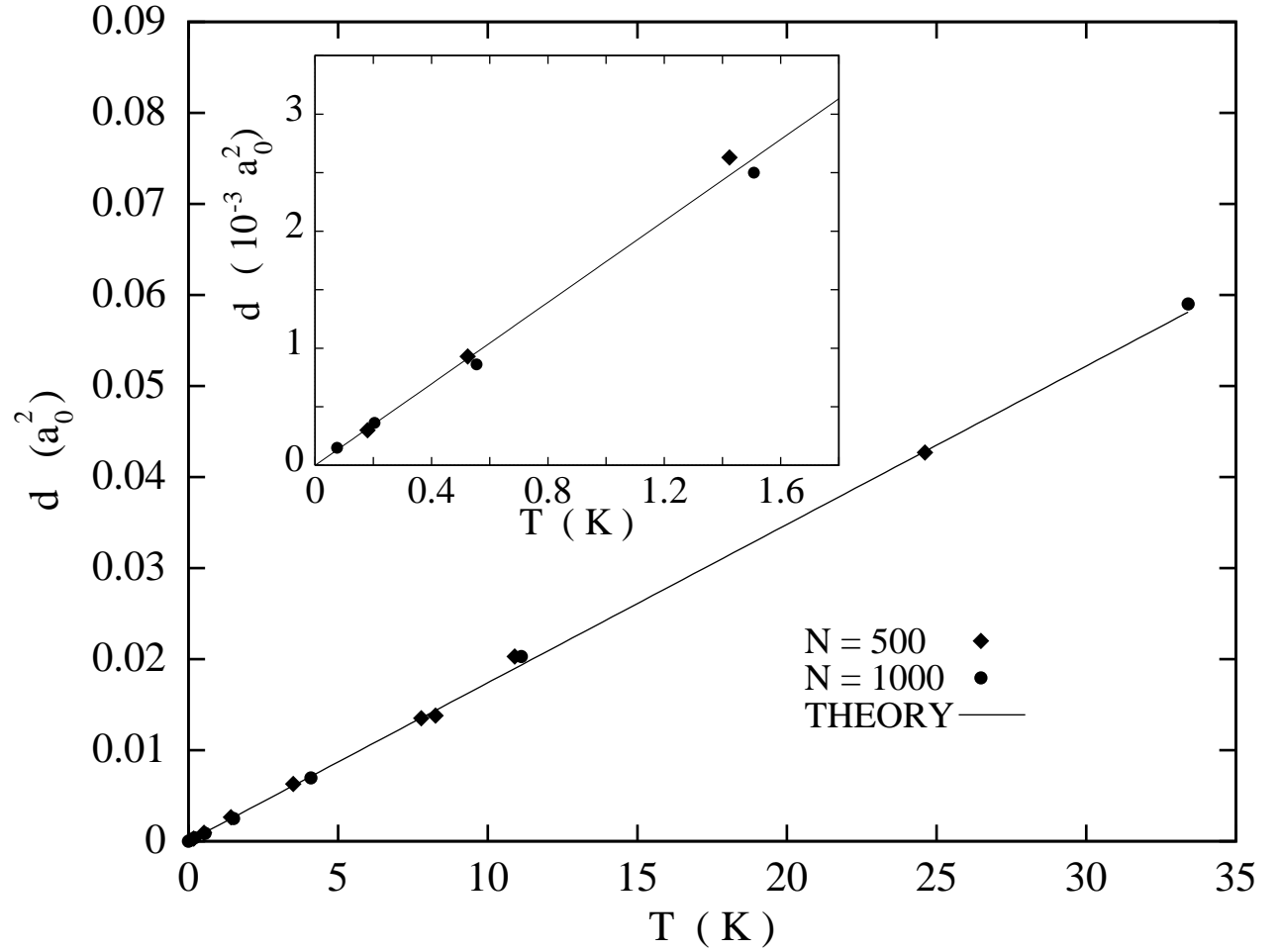


Figure 7: d versus T for several confined states in the upper group compared with the harmonic prediction. The inset figure shows the low-temperature data in more detail. Adapted from [19].

valley's depth Φ_0 and vibrational frequency spectrum $g(\omega)$. They made the following observations about the valleys:

(1) The depths of the valleys occupied by the upper states all lie in a very narrow range,

$$\Phi_0/N = -0.01352 \pm 0.00002 \text{ Ry/particle}, \quad (7)$$

and they all have virtually the same normal mode frequency spectrum independent of the valley or even N . The normal mode spectra for five such valleys are shown in Figure 8. Since the normal mode frequencies for different valleys are so similar, it comes as no surprise that the three principal moments of the frequency distribution, Θ_{-2} , Θ_0 , and Θ_2 , defined by

$$\begin{aligned} k_B \Theta_{-2} &= \left[\frac{1}{3} \langle (\hbar\omega)^{-2} \rangle \right]^{-1/2} \\ \ln k_B \Theta_0 &= \langle \ln \hbar\omega \rangle \\ k_B \Theta_2 &= \left[\frac{5}{3} \langle (\hbar\omega)^2 \rangle \right]^{1/2}, \end{aligned} \quad (8)$$

where $\langle \rangle$ denotes an average over the normal mode spectrum, also vary little from valley to valley. (These averages always exclude the three zero-frequency modes that correspond to center of mass motion.) Their values fall in the ranges

$$\begin{aligned} \Theta_{-2} &= 114 \pm 4 \text{ K} \\ \Theta_0 &= 98.7 \pm 0.1 \text{ K} \\ \Theta_2 &= 154.0 \pm 0.1 \text{ K}. \end{aligned} \quad (9)$$

The larger uncertainty in Θ_{-2} arises because Θ_{-2} is very sensitive to the lowest part of the frequency distribution, and thus to a small system size.

(2) The equilibrium configuration of particles at the bottom of a valley is called a *structure*; Clements and Wallace denote the pair distribution function for a structure $G_\gamma(r)$, where γ labels the valley in which the structure lies. They cooled several confined states in the upper group to find the corresponding structures and found that they all had very nearly the same $G_\gamma(r)$, as illustrated in Figure 9. The fluctuations at small N gradually vanish as N increases. (This figure includes one valley at $N = 168$ which was studied in early exploratory calculations, but which was not used in the final work except at this point.)

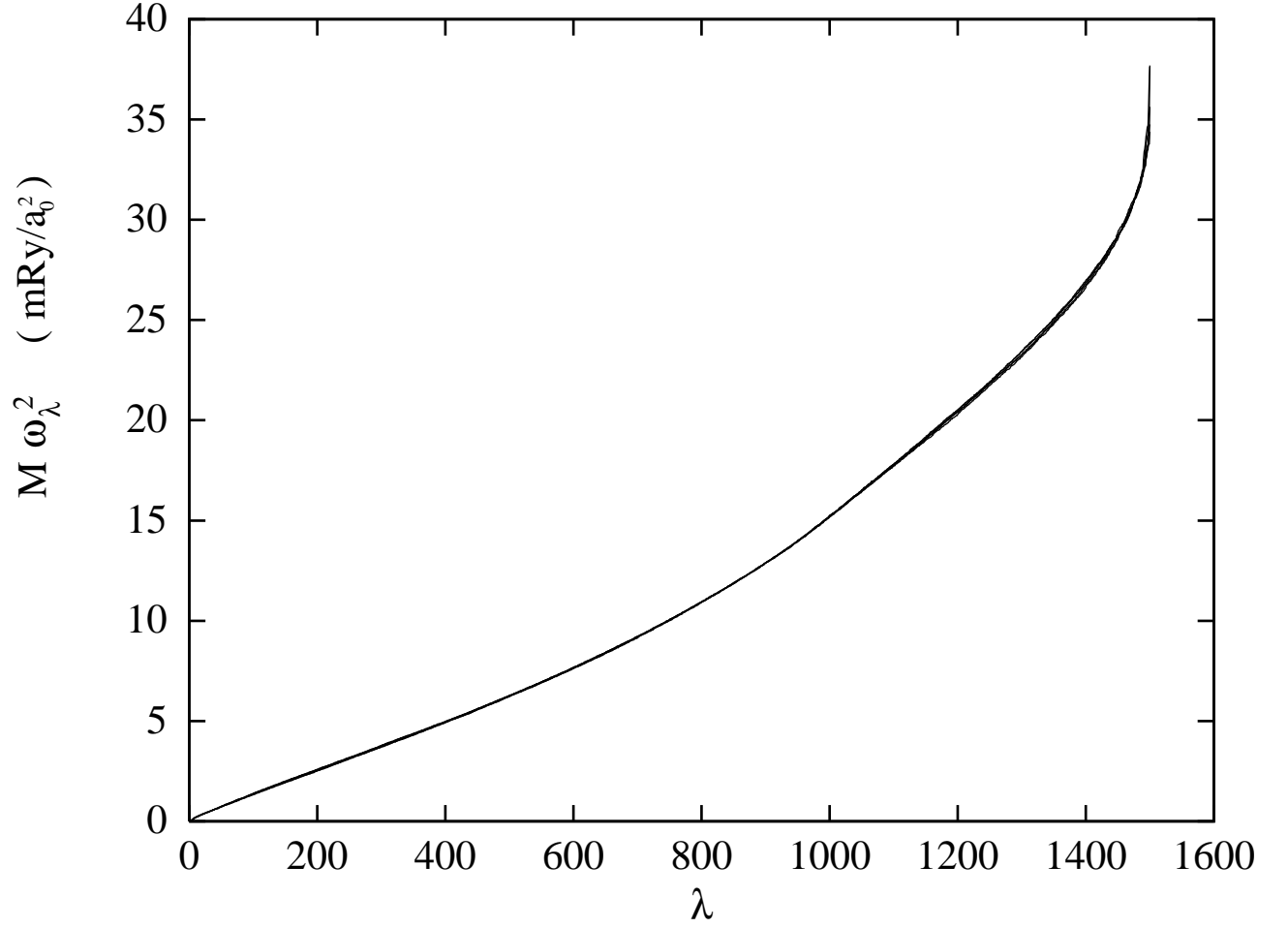


Figure 8: The normal mode spectra for five different valleys occupied by upper equilibrium states. Eigenvalues are given as $M\omega_\lambda^2$ where M is the atomic mass of sodium and λ is a label that counts the eigenvalues. From [19].

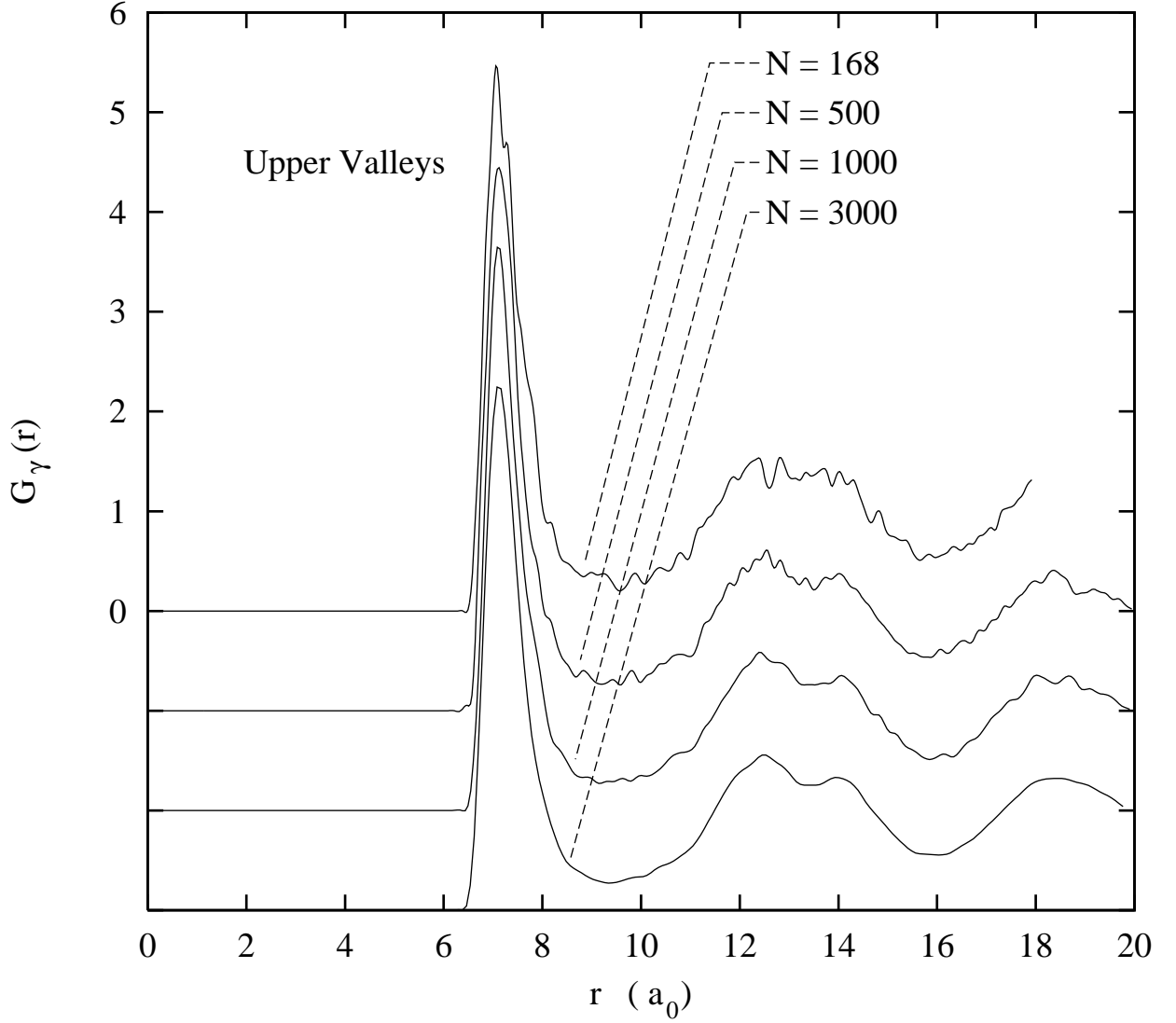


Figure 9: Structure pair distribution functions $G_\gamma(r)$ for four different valleys occupied by states from the upper group. As N increases the small wiggles vanish. Adapted from [20].

(3) The universal $G_\gamma(r)$ for the valleys occupied by confined upper states exhibits a split second peak (as is seen most clearly in the $N = 3000$ plot in Figure 9), just as $g(r)$ for the states from the lower group do [see point (6) above], but with the first subpeak *higher* than the second. Experiments on Ni, Co, Cr, Fe, and Mn have identified this as a signature of an amorphous structure [36, 37, 38, 39].

(4) Clements and Wallace also constructed the set of Voronoi polyhedra for each structure, and from this they computed the statistical distributions of two coordination numbers: The number of faces per polyhedron, and the angle between lines joining a particle to its Voronoi neighbors. They found that these distributions were universal across all of the structures found by cooling states in the upper group.

(5) The valleys occupied by states in the lower group, on the other hand, do not exhibit universality in any of the properties measured: Their depths, normal mode distributions, structure pair distribution functions, and distributions of coordination numbers vary substantially from valley to valley.

(6) The peaks in $G_\gamma(r)$ for any valley occupied by a state from the lower group are more numerous and narrow than the peaks in the universal $G_\gamma(r)$ of the valleys occupied by the upper states, while the peaks in the bcc crystal $G_{\text{bcc}}(r)$ are more narrow still.

These results provide strong evidence that the many-body potential surface of sodium contains two distinct classes of valleys: the valleys in the first class exhibit universality in a wide variety of properties, while the valleys in the second class don't. The potential surface is dominated by valleys of the first class, and equilibrium states from the upper group are either confined to a single valley of this class or move primarily among such valleys. (That the first class dominates is shown by the fact that the system almost always equilibrates to an upper state first.) Since the upper states lie along the same energy curve as the liquid states and $g(r)$ for the upper states evolves continuously into $g(r)$ for the liquid as T increases, the statistical mechanics of the liquid is determined primarily by the properties of the first class of valleys. We have less conclusive evidence that these valleys are approximately harmonic [points (1) and (6) about the states] and that the structures in the second class of valleys are less rigidly ordered than the bcc crystal structure but more rigidly ordered than the structures in the first class of valleys [points (3) and (6) about the valleys]. Thus we conclude that the valleys in the first class are random, and those in the second class are symmetric. (The rms vibrational frequency and period for a “typical” many-body valley in

sodium in Subsection 3.1 were computed for the random valleys.) Remnant symmetry in the lower valleys is also consistent with their lower Φ_0 . In this system, the Φ_0 values of the symmetric valleys range from the value for the bcc valley up to the universal value for the random valleys; symmetric valleys could conceivably have even higher Φ_0 values, but none were found in this study. Thus we conclude that our general picture of the potential surface of a monatomic liquid is rather well confirmed for this element.

3.2.2 Lennard-Jones argon

We conducted a less exhaustive study of Lennard-Jones argon [21] in which we reproduced some of the results described above for sodium. One difficulty we found with LJ argon is an interesting instability: The system has a threshold density which lies between the experimental densities of liquid Ar and fcc crystal Ar at 1 bar, and if one attempts to cool the system at a constant density below this threshold, the system will collapse spontaneously until the threshold is reached. This limits one's ability to study densities below the threshold at low temperatures. Nonetheless, we were able to explore many valleys at the threshold density using the same technique as in sodium, and we found a group of states lying above those occupying the fcc valley on a $\langle\Phi/N\rangle$ versus $\langle\mathcal{K}/N\rangle$ graph, as in point (1) for sodium. The valleys occupied by these states exhibit the following properties:

- (1) They pass both tests of harmonicity (points (1) and (6) for states of sodium).
- (2) Equilibrium states that move among these valleys are continuous with the liquid states on the $\langle\Phi/N\rangle$ versus $\langle\mathcal{K}/N\rangle$ graph.
- (3) The values of Φ_0/N for all valleys lie in the same narrow range.

Given our experience with sodium, we conclude tentatively that we have found the random valleys in Lennard-Jones argon. Thus the rms vibrational frequency and period for a “typical” many-body valley in argon in Subsection 3.1 were computed from these valleys. Further tests on argon and other liquids will be considered in Section 6.

4 Equilibrium statistical mechanics

Now let us use the picture to develop a first order approximation to the statistical mechanics of a monatomic liquid. The specific heat data suggest

that the departures from harmonicity in the liquid's Hamiltonian may be treated as higher-order perturbations, at least for purposes of equilibrium statistical mechanics, and we shall keep this in mind as we investigate the Hamiltonian and compute thermodynamic quantities. Corrections beyond the leading order will be considered as we proceed.

4.1 The Hamiltonian

The general Hamiltonian for the system is written

$$H = \sum_{Ki} \frac{p_{Ki}^2}{2M} + \Phi(\{\mathbf{r}_K\}) \quad (10)$$

where the index K labels the particles, i labels the components of the position or momentum of a single particle, M is the mass of one atom, and Φ is the many-body potential. We have argued that the potential surface is dominated by a collection of nearly harmonic valleys; let these valleys be labeled with the index γ , which presumably runs from 1 to approximately w^N . We wish to consider the form of the Hamiltonian when the system is localized in a particular valley. The coordinates of the particles at the valley bottom will be denoted $\{\mathbf{R}_K(\gamma)\}$, and we define

$$\mathbf{u}_K(\gamma) = \mathbf{r}_K - \mathbf{R}_K(\gamma) \quad (11)$$

to be the displacement of the K th particle from its equilibrium position. The many-body potential in the valley will be denoted Φ_γ and can be expanded as

$$\Phi_\gamma(\{\mathbf{u}_K(\gamma)\}) = \Phi_0(\gamma) + \frac{1}{2} \sum_{Ki, Lj} \Phi_{Ki, Lj}(\gamma) u_{Ki}(\gamma) u_{Lj}(\gamma) + \Phi_A(\gamma) \quad (12)$$

where

$$\Phi_0(\gamma) = \Phi(\{\mathbf{R}_K\}) = \Phi(\{\mathbf{u}_K = \mathbf{0}\}), \quad (13)$$

$$\Phi_{Ki, Lj}(\gamma) = \frac{\partial^2 \Phi}{\partial r_{Ki} \partial r_{Lj}}(\{\mathbf{R}_K\}), \quad (14)$$

and $\Phi_A(\gamma)$ contains all of the higher order contributions to Φ_γ . $\Phi_{Ki, Lj}(\gamma)$ is called the “dynamical matrix” of the potential valley. The Hamiltonian in the valley will be denoted H_γ and can now be written

$$H_\gamma = \Phi_0(\gamma) + H_H(\gamma) + \Phi_A(\gamma) \quad (15)$$

where

$$H_H(\gamma) = \sum_{Ki} \frac{p_{Ki}^2}{2M} + \frac{1}{2} \sum_{Ki,Lj} \Phi_{Ki,Lj}(\gamma) u_{Ki}(\gamma) u_{Lj}(\gamma) \quad (16)$$

is the harmonic contribution. An appropriate orthogonal transformation replaces the $\mathbf{u}_K(\gamma)$ with new coordinates $q_\lambda(\gamma)$ that diagonalize the dynamical matrix:

$$H_H(\gamma) = \sum_{\lambda} \left(\frac{p_{\lambda}^2}{2M} + \frac{1}{2} M \omega_{\lambda}^2(\gamma) q_{\lambda}^2(\gamma) \right). \quad (17)$$

This also defines the normal mode frequencies $\omega_{\lambda}(\gamma)$. If the system contains N particles, then λ ranges from 1 to $3N$. If the valley happens to be random, the Hamiltonian simplifies further; since the random valleys all have the same depth and normal mode spectrum, the label γ on the frequencies and Φ_0 can be dropped, so

$$H_{\gamma} = \Phi_0 + H_H(\gamma) + \Phi_A(\gamma) \quad (18)$$

where

$$H_H(\gamma) = \sum_{\lambda} \left(\frac{p_{\lambda}^2}{2M} + \frac{1}{2} M \omega_{\lambda}^2 q_{\lambda}^2(\gamma) \right). \quad (19)$$

The Hamiltonian in Equation (15), with the harmonic part given by Equation (17), is the starting point of our treatment of equilibrium statistical mechanics. Note that these equations describe a restriction of the full Hamiltonian, Equation (10), to a single potential valley, so they are defined only within that valley. The term Φ_A in the potential may describe any sort of anharmonicity within the valley, but its main contribution is expected to occur at the edges of the valley, where the potential presumably flattens out (and departs from strict harmonic behavior) before dipping down into a neighboring valley.

4.2 The partition function

We will now compute the quantum mechanical partition function and the resulting thermodynamics, excluding exchange effects. (A quantum treatment is necessary for light elements including Li, Ne, and Be, but without exchange effects this treatment will be insufficient for describing liquid He.) We will also display the classical limits of our results; a fully classical development may be found in [16].

The partition function may be written

$$Z = \text{Tr}(e^{-\beta H}) = \sum_E g(E) e^{-\beta E} \quad (20)$$

where E ranges over the eigenvalues of the Hamiltonian H and $g(E)$ is a degeneracy factor which equals the dimension of the eigenspace corresponding to E . If the Hamiltonian described a single harmonic valley of unbounded spatial extent with normal mode frequencies ω_λ , the eigenvalues would take the form

$$E = \sum_\lambda \left(n_\lambda + \frac{1}{2} \right) \hbar \omega_\lambda \quad (21)$$

where the n_λ are arbitrary nonnegative integers. We have argued that the true potential is dominated overwhelmingly by a single class of nearly harmonic valleys, the random valleys, all of which have the same normal mode spectrum; therefore, let us approximate the eigenvalues of the harmonic part of the actual Hamiltonian, Equation (17), with values of the form given in Equation (21) using the universal random valley normal mode spectrum; it then remains to determine the degeneracy of each. Our approximation suggests the existence of eigenfunctions of H which are largely confined to individual valleys; clearly there would be approximately w^N of these for each eigenvalue, one per valley, and these would be approximately orthogonal (because they are almost spatially disjoint), hence approximately linearly independent. Thus we suggest $g(E) \approx w^N$ independent of E , or

$$\begin{aligned} Z &\approx \sum_{\{n_\lambda\}} w^N \exp \left(-\beta \left[\Phi_0 + \sum_\lambda \left(n_\lambda + \frac{1}{2} \right) \hbar \omega_\lambda \right] \right) \\ &= w^N e^{-\beta \Phi_0} \sum_{\{n_\lambda\}} \prod_\lambda \exp \left[-\beta \left(n_\lambda + \frac{1}{2} \right) \hbar \omega_\lambda \right] \\ &= w^N e^{-\beta \Phi_0} \prod_\lambda \sum_n \exp \left[-\beta \left(n + \frac{1}{2} \right) \hbar \omega_\lambda \right] \\ &= w^N e^{-\beta \Phi_0} \prod_\lambda \frac{e^{-\frac{1}{2}\beta \hbar \omega_\lambda}}{1 - e^{-\beta \hbar \omega_\lambda}}. \end{aligned} \quad (22)$$

This is the approximate partition function for the liquid. In the classical limit ($\hbar \omega_\lambda \ll k_B T$ for all λ),

$$Z \approx w^N e^{-\beta \Phi_0} \prod_\lambda (\beta \hbar \omega_\lambda)^{-1}. \quad (23)$$

We have made three noteworthy approximations in calculating Z : First, we have neglected the contributions from the symmetric and crystalline valleys. This is a superb approximation, however, since the random valleys vastly outnumber the other two types. Second, we have neglected the term Φ_A in the Hamiltonian (15). Third, in using energy eigenvalues of the form (21) we have implicitly extended a single potential valley throughout all of configuration space, failing to take into account its limited spatial extent; we have thus neglected the existence of *boundaries* of the valleys. These last two approximations are more significant, and their effects will be included in our subsequent calculations.

4.3 Thermodynamic state functions

To each thermodynamic state function X we will append a term of the form X_{AB} representing the corrections due to anharmonicity and boundary effects, as discussed immediately above, without further comment. The Helmholtz free energy is

$$\begin{aligned} F &= -k_B T \ln Z \\ &= \Phi_0 - Nk_B T \ln w + \sum_{\lambda} \left[\frac{1}{2} \hbar \omega_{\lambda} - k_B T \ln(n_{\lambda} + 1) \right] + F_{AB} \end{aligned} \quad (24)$$

where

$$n_{\lambda} = \frac{1}{e^{\beta \hbar \omega_{\lambda}} - 1}, \quad (25)$$

the entropy is

$$\begin{aligned} S &= - \left(\frac{\partial F}{\partial T} \right)_V \\ &= Nk_B \ln w + k_B \sum_{\lambda} [(n_{\lambda} + 1) \ln(n_{\lambda} + 1) - n_{\lambda} \ln n_{\lambda}] + S_{AB} \end{aligned} \quad (26)$$

where n_{λ} is defined as before, and the internal energy is

$$\begin{aligned} U &= F + TS \\ &= \Phi_0 + \sum_{\lambda} \left(n_{\lambda} + \frac{1}{2} \right) \hbar \omega_{\lambda} + U_{AB}. \end{aligned} \quad (27)$$

Finally, the constant-volume specific heat is

$$\begin{aligned} C_V &= \left(\frac{\partial U}{\partial T} \right)_V \\ &= k_B \sum_{\lambda} \left[n_{\lambda}(n_{\lambda} + 1)(\beta \hbar \omega_{\lambda})^2 \right] + C_{AB}. \end{aligned} \quad (28)$$

It is convenient to express the state functions in the classical limit in terms of the temperature Θ_0 defined as in Subsection 3.2 by

$$\ln k_B \Theta_0 = \frac{\sum_{\lambda} \ln \hbar \omega_{\lambda}}{3N}. \quad (29)$$

Using this definition, in the limit $\hbar \omega_{\lambda} \ll k_B T$ for all λ we find

$$F = \Phi_0 - Nk_B T \ln w - 3Nk_B T \ln(T/\Theta_0) + F_{AB}, \quad (30)$$

$$S = Nk_B \ln w + 3Nk_B [\ln(T/\Theta_0) + 1] + S_{AB}, \quad (31)$$

$$U = \Phi_0 + 3Nk_B T + U_{AB}, \quad (32)$$

$$C_V = 3Nk_B + C_{AB}. \quad (33)$$

4.4 Comparison with experiment

All comparisons with experimental data will be done in the classical limit. First, we derive the expression for entropy of melting. The entropy for a monatomic harmonic crystal has the same form as the liquid, Equation (31), without the $Nk_B \ln w$ term since the system resides in a single potential valley. Let the superscript l denote quantities of the liquid and c those of the crystal; then

$$\begin{aligned} S^l &= Nk_B \ln w + 3Nk_B [\ln(T/\Theta_0^l) + 1] + S_{AB}^l + S_E^l \\ S^c &= 3Nk_B [\ln(T/\Theta_0^c) + 1] + S_A^c + S_E^c \end{aligned} \quad (34)$$

where S_E is the valence electronic contribution to the entropy (note that the crystal's entropy has anharmonic corrections but no boundary corrections), so the entropy of melting at constant density ΔS is given by

$$\begin{aligned} \Delta S &= S^l(T_m) - S^c(T_m) \\ &= Nk_B \ln w + 3Nk_B \ln(\Theta_0^c/\Theta_0^l) + (S_{AB}^l - S_A^c) + (S_E^l - S_E^c). \end{aligned} \quad (35)$$

Let us consider a normal melting element. Since its electronic structure is not changed significantly upon melting, it is reasonable to suspect that $S_E^l \approx S_E^c$, so assuming anharmonic and boundary effects are small, the entropy of melting is dominated by the first two terms, the second of which depends strongly on the individual element and the first of which may or may not depend strongly, depending on how w varies between different substances. The experimental data from Subsection 2.1.2 reveal that $\Delta S = 0.8 Nk_B$ for all nearly-free-electron metals with a small scatter; the only term in Equation (35) that could reasonably be considered universal and thus account for these data is the first, assuming w is itself universal and $\ln w = 0.8$. That in turn implies that $\Theta_0^c \approx \Theta_0^l$ for normal melters, with the departures from strict equality, along with anharmonic, boundary, and electronic entropy contributions, accounting for the scatter in ΔS . We have verified the prediction $\Theta_0^c \approx \Theta_0^l$ for sodium and Lennard-Jones argon, both of which are normal melters; for sodium in the bcc crystal phase [19]

$$\Theta_0 = 99.65 \text{ K}, \quad (36)$$

which is quite close to $\Theta_0 = 98.7 \pm 0.1 \text{ K}$ for the liquid [Equation (9)]. For argon, $\Theta_0 = 42.5 \text{ K}$ for the liquid at $\rho = 1.6000 \text{ g/cm}^3$, and $\Theta_0 = 43.4 \text{ K}$ for the fcc crystal at the same density [21]. We also predict that the much higher ΔS values of the anomalous melters can be accounted for mainly from the different values of Θ_0 and S_E for the two phases, both because of their very different electronic structures, plus the usual small anharmonic and boundary effects.

Second, Wallace [16] has compared Equations (34) (neglecting anharmonic and boundary terms) to experimental entropy data for six nearly-free-electron metals; the criteria used to select the six elements, and the details of the correction of the data for density changes, are given in [16]. Figure 10 shows the theoretical prediction for the entropy of mercury in crystal and liquid phases, over a temperature range from below T_m to $3.2 T_m$, compared to experimental data. The agreement is most encouraging. The differences between experimental and theoretical entropy as a function of T/T_m for all six elements are shown in Figure 11. The differences fall within the expected errors in the analysis, as discussed in [16]. Recall that all thermodynamic functions are derived from a single potential, taken in this case to be the free energy, which has both a zero-temperature part, Φ_0 , and a thermal part (see Equation (24) or (30)); because of this, it suffices to compare one function (in

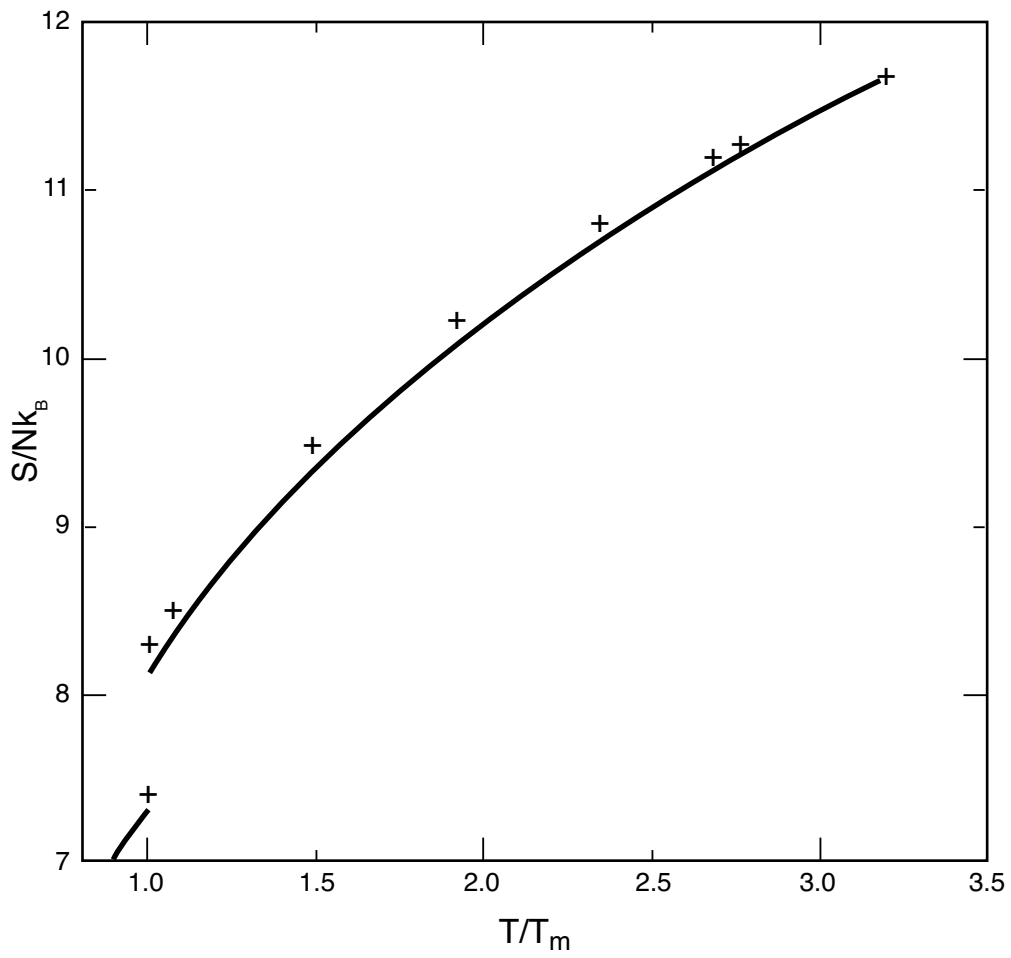


Figure 10: Theoretical prediction of the entropy of mercury in crystal and liquid phases (curve) compared with experimental data (crosses). Adapted from [16].

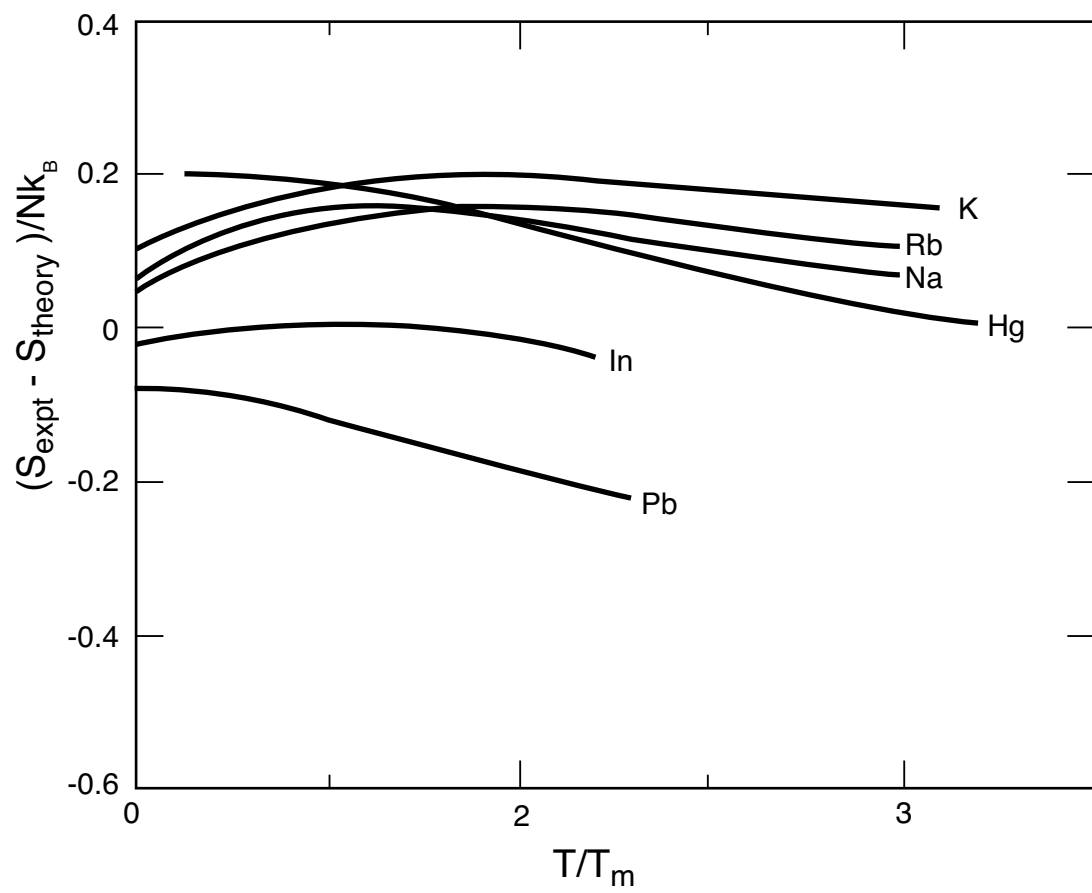


Figure 11: Difference between experimental and theoretical entropy for six liquid metals. Adapted from [16].

this case, entropy) with experiment to guarantee the accuracy of the thermal part of our entire thermodynamic treatment.

To check the zero-temperature part of our thermodynamics, we consider one further point of contact with experiment. As Wallace has shown in [16], the potential minima of the liquid and crystal, corrected for density differences, should obey the relation

$$\Phi_0^l(\rho_{lm}) - \Phi_0^c(\rho_{lm}) \approx T_m \Delta S \quad (37)$$

where ρ_{lm} is the density of the liquid at melt. This assumes that both liquid and crystal obey the harmonic relation $\langle \Phi \rangle = \Phi_0 + (3/2)Nk_B T$, so the difference in $U = \langle \Phi \rangle + (3/2)Nk_B T$ equals the difference in Φ_0 . However, as noted in [19], experiments on sodium have determined that $T_m \Delta S = 1.7$ mRy/atom, while MD calculations (Figure 5) show that the difference in potential minima between the random valleys and the bcc valley is roughly 0.92 mRy/atom, which is of the right order of magnitude but is 46% smaller than experiment. The reason for this discrepancy is easy to find; as can be seen in Figure 5 and more clearly in Figure 4 of [19], which plots the states in the random valleys together with the liquid states, the slope of the line followed by the states increases at higher T , so $\langle \Phi \rangle$ does not obey the harmonic relation. If one uses the values of $\langle \Phi \rangle$ from Figure 4 of [19] at melt, one finds that the difference in U is in fact 1.7 mRy/atom. We will return to this anharmonicity in Section 6.

5 Nonequilibrium statistical mechanics

It is not often enough emphasized that equilibrium statistical mechanics and its nonequilibrium counterpart ultimately have the same starting point, the Hamiltonian of the system, although they make use of the Hamiltonian in very different ways. Both begin with a decomposition of the Hamiltonian into “free” and “transition” terms, where the “free” term is the more tractable of the two and can be fairly readily diagonalized. In equilibrium statistical mechanics, the entire Hamiltonian contributes to the partition function, but often the contribution of the transition term cannot be computed exactly, so its effects are usually included as a perturbative approximation. Nonequilibrium statistical mechanics, on the other hand, treats the system as executing transitions between the states that diagonalize the free part of the Hamiltonian, with the transition term determining cross sections and

transition rates. In a gas, for example, the free part of the Hamiltonian describes N -body free motion, while the transition part is responsible for interparticle interactions. An equilibrium treatment of a gas portrays it as an ideal gas with perturbations away from ideal behavior produced by the interaction terms; a nonequilibrium treatment via the Boltzmann equation portrays the gas as executing transitions between many-body free motion states by means of collisions, which are ultimately mediated by the same interaction terms responsible for perturbations in the equilibrium treatment. The liquid is analogous: The Hamiltonian decomposes into a “free” term, which is Φ_0 plus the harmonic term from Equation (17), and a “transition” term, which consists of Φ_A from Equation (15) plus the presence of boundaries. The equilibrium statistical mechanics of the liquid, as we have seen, is dominated by the “free” term, although the other terms introduce corrections; and nonequilibrium statistical mechanics ultimately should treat the liquid as executing transits between states confined to individual valleys, with transits mediated by the boundary term of the Hamiltonian. (This fact connects transits in nonequilibrium mechanics to the boundary corrections in equilibrium mechanics; see Section 6.) Thus transits, which do not appear in the equilibrium results at all to lowest order, will play a central role in understanding the liquid’s nonequilibrium behavior. Because of this we begin by writing the position of the K th particle in the liquid as

$$\mathbf{r}_K(t) = \mathbf{R}_K(t) + \mathbf{u}_K(t) \quad (38)$$

where $\mathbf{R}_K(t)$ is the location of the center about which the particle oscillates between transits and $\mathbf{u}_K(t)$ is motion about that center. Then $\mathbf{R}_K(t)$ changes only when a transit involving particle K takes place. (Compare Equation (11).) This decomposition, which is motivated by a corresponding decomposition of the Hamiltonian, is the starting point of our nonequilibrium treatment.

We will work in the linear regime, in which the coefficients determining the system’s nonequilibrium response (self-diffusion, bulk viscosity, shear viscosity, thermal conductivity, etc.) are related to equilibrium time-correlation functions by expressions of the Green-Kubo form [40]; thus our goal is to understand the physics behind the appropriate correlation functions. We will perform a sample calculation of two simple correlation functions, and then we will proceed to the very important velocity autocorrelation function, which determines the self-diffusion coefficient. We will work in the classical limit; quantum aspects will be discussed in Section 6.

5.1 Correlation functions in the absence of transits

An important part of this work involves calculating correlation functions of harmonically varying quantities, so we will first show such a computation by considering the one-particle functions $\langle \mathbf{u}(t) \cdot \mathbf{u}(0) \rangle$ and $\langle \mathbf{v}(t) \cdot \mathbf{v}(0) \rangle$ in the simplest situation, when the temperature is sufficiently low that the system remains in a single valley without transits. (We recall from Subsection 3.1 that this is below roughly 30 K for sodium and 17.1 K for Lennard-Jones argon.) Ultimately we will be comparing these results with MD simulations, in which the center of mass of the system is stationary; in this case, only $N - 1$ of the particles' positions are independent, so we define correlation functions as averages over particles with that restriction, and we divide by $N - 1$, not N , to take into account the reduced number of independent degrees of freedom. We consider the position correlation function first.

$$\begin{aligned} \langle \mathbf{u}(t) \cdot \mathbf{u}(0) \rangle &\equiv \frac{1}{N-1} \sum_K \langle \mathbf{u}_K(t) \cdot \mathbf{u}_K(0) \rangle \\ &= \frac{1}{N-1} \sum_{Ki} \langle u_{Ki}(t) u_{Ki}(0) \rangle. \end{aligned} \quad (39)$$

Let the orthogonal transformation from the original coordinates to the normal mode coordinates be denoted $w_{Ki,\lambda}$, so

$$u_{Ki}(t) = \sum_{\lambda} w_{Ki,\lambda} q_{\lambda}(t), \quad (40)$$

where the normal modes are denoted q_{λ} as in Subsection 4.1; then

$$\begin{aligned} \langle \mathbf{u}(t) \cdot \mathbf{u}(0) \rangle &= \frac{1}{N-1} \sum_{Ki,\lambda,\lambda'} \langle w_{Ki,\lambda} w_{Ki,\lambda'} q_{\lambda}(t) q_{\lambda'}(0) \rangle \\ &= \frac{1}{N-1} \sum_{\lambda} \langle q_{\lambda}(t) q_{\lambda}(0) \rangle. \end{aligned} \quad (41)$$

Because the potential of the system is invariant under translations, three of the q_{λ} (the components of the center of mass) are zero-frequency modes; since these modes are not excited by assumption, λ ranges from 1 to $3N - 3$ over the nonzero modes. Now

$$\langle q_{\lambda}(t) q_{\lambda}(0) \rangle \equiv \left\langle \left\{ e^{-i\mathcal{L}t} q_{\lambda} \right\} q_{\lambda} \right\rangle \quad (42)$$

where \mathcal{L} is the Liouville operator for the system, so in our harmonic approximation

$$\begin{aligned}\langle q_\lambda(t) q_\lambda(0) \rangle &= \left\langle \left\{ q_\lambda \cos(\omega_\lambda t) + \frac{p_\lambda}{M\omega_\lambda} \sin(\omega_\lambda t) \right\} q_\lambda \right\rangle \\ &= \langle q_\lambda^2 \rangle \cos(\omega_\lambda t) + \frac{\langle q_\lambda p_\lambda \rangle}{M\omega_\lambda} \sin(\omega_\lambda t)\end{aligned}\quad (43)$$

where $\{\omega_\lambda\}$ is the set of normal mode frequencies of a random valley. (The system is overwhelmingly likely to be in a random valley because such valleys dominate the potential surface.) The two averages are easily calculated in the canonical ensemble,

$$\langle q_\lambda^2 \rangle = \frac{k_B T}{M\omega_\lambda^2}, \quad \langle q_\lambda p_\lambda \rangle = 0, \quad (44)$$

and the final result is

$$\langle \mathbf{u}(t) \cdot \mathbf{u}(0) \rangle = \frac{1}{N-1} \frac{k_B T}{M} \sum_\lambda \frac{\cos(\omega_\lambda t)}{\omega_\lambda^2}. \quad (45)$$

(Note that, aside from the fact that $\mathbf{u}(0)$ and $\mathbf{u}(t)$ would appear symmetrically in the definition of the correlation function, the quantum calculation proceeds identically to its classical counterpart until Equation (44).) Since $\mathbf{v}(t) = \dot{\mathbf{u}}(t)$ in the absence of transits, a similar line of reasoning leads to

$$\langle \mathbf{v}(t) \cdot \mathbf{v}(0) \rangle = \frac{1}{N-1} \frac{k_B T}{M} \sum_\lambda \cos(\omega_\lambda t). \quad (46)$$

These results, which have the same form as the corresponding results for a harmonic crystal, will serve as a reference point for the work of the next subsection.

5.2 Velocity autocorrelation function and diffusion coefficient

Now we will consider the velocity autocorrelation function $Z(t)$, defined by

$$Z(t) = \frac{1}{3} \langle \mathbf{v}(t) \cdot \mathbf{v}(0) \rangle, \quad (47)$$

which determines the self-diffusion coefficient D through the Green-Kubo relation [40]

$$D = \int_0^\infty Z(t) dt. \quad (48)$$

We predict from Equation (46) that at sufficiently low temperatures

$$Z(t) = \frac{1}{3N-3} \frac{k_B T}{M} \sum_\lambda \cos(\omega_\lambda t), \quad (49)$$

or in terms of $\hat{Z}(t) \equiv Z(t)/Z(0)$,

$$\hat{Z}(t) = \frac{1}{3N-3} \sum_\lambda \cos(\omega_\lambda t). \quad (50)$$

It is not at all clear, however, how this result will be modified at higher temperatures by transits; certainly even an approximate solution to the system's equations of motion seems well out of reach. In [23] we argued that trying to understand the motion of the system in terms of a normal mode decomposition would be unhelpful once transits begin to occur for the following reasons: Over a broad range of temperatures, we suspect that any given particle will participate in a transit roughly once per mean vibrational period (this will be verified below), so each particle will experience roughly ten transits by its neighbors per period. Each such transit changes the many-body valley in which the system lies, thus changing the particular normal mode decomposition in which the coordinates of all the particles are expressed. Perhaps such a change would minimally affect the coordinates of far away particles, but it should certainly have a substantial effect on the coordinates of the near neighbors. In response to this, one could instead suggest that the normal mode picture needs only to be supplemented, not replaced, and this line of reasoning has been followed most notably in some INM work (for example, [9, 10]); however, that work has focused not on constructing an explicit model for the system's motion while transiting, but on modeling the effects of transits on Equation (49) directly in the general form suggested by Zwanzig [41]. If we must resort to models, we strongly prefer developing a model of the actual motion of the particles in the liquid, transits included, and then calculating $Z(t)$ from there, because we believe that the important thing to be understood is the motion, not just the behavior of one correlation coefficient, and because such a model can then be used to calculate any single-particle correlation coefficient one chooses. Thus in

[23] we proposed a mean-atom-trajectory model, which consists of a single average particle in the liquid periodically transiting between single-particle equilibrium positions while executing harmonic motion between transits. We then incorporated into this model the essential features one expects from an actual solution to the equations of motion of the system, as shown below.

Since each transit carries the system with overwhelming likelihood between random valleys, it is sensible to model the average particle's motion between transits in terms of oscillations at the random valley frequency distribution, or

$$\begin{aligned}\mathbf{r}(t) &= \mathbf{R} + \mathbf{u}(t) \\ &= \mathbf{R} + \sum_{\lambda} \mathbf{w}_{\lambda} \sin(\omega_{\lambda} t + \alpha_{\lambda})\end{aligned}\tag{51}$$

where \mathbf{R} and $\mathbf{u}(t)$ are the mean-atom equivalents of \mathbf{R}_K and $\mathbf{u}_K(t)$ from Equation (38). (Between transits \mathbf{R} has no time dependence.) Now the parameters \mathbf{w}_{λ} and α_{λ} in $\mathbf{u}(t)$ remain to be determined. Let us assume that the values of the phases α_{λ} are randomly distributed among the particles; then one calculates $Z(t)$ from Equation (51) by differentiating to find $\mathbf{v}(t)$, computing the product $\mathbf{v}(t) \cdot \mathbf{v}(0)$, and averaging over each of the α_{λ} separately; the result is

$$Z(t) = \frac{1}{6} \sum_{\lambda} |\mathbf{w}_{\lambda}|^2 \omega_{\lambda}^2 \cos(\omega_{\lambda} t).\tag{52}$$

Equation (52) becomes Equation (49) with the choice

$$\mathbf{w}_{\lambda} = \sqrt{\frac{1}{N-1} \frac{2k_B T}{M \omega_{\lambda}^2}} \hat{\mathbf{w}}_{\lambda}\tag{53}$$

where $\hat{\mathbf{w}}_{\lambda}$ is an arbitrarily chosen unit vector. Thus Equation (51) with the phases α_{λ} randomly chosen and \mathbf{w}_{λ} given by Equation (53), with the unit vectors $\hat{\mathbf{w}}_{\lambda}$ also randomly chosen, constitute our mean-atom-trajectory model between transits. (A brief calculation shows that this model also yields the correct result for $\langle \mathbf{u}(t) \cdot \mathbf{u}(0) \rangle$ from Equation (45).)

Next we must determine the effect of transits on the parameters in $\mathbf{r}(t)$, and that requires an explicit model of both the transit of an average particle and the rate at which transits occur. First, the transit process itself. We assume that the transit occurs instantaneously (the particle simply crosses the surface separating distinct valleys), so it must conserve both the particle's position $\mathbf{r}(t)$ and velocity $\mathbf{v}(t)$. To be more specific, we assume that the

transit occurs in the forward direction, so that the center of the new valley lies an equal distance away from the particle but on the opposite side from the center of the old valley. Let $\mathbf{r}^{\text{before}}(t)$, $\mathbf{R}^{\text{before}}$, and $\mathbf{u}^{\text{before}}(t)$ be the position parameters from Equation (51) before the transit, and let $\mathbf{r}^{\text{after}}(t)$, $\mathbf{R}^{\text{after}}$, and $\mathbf{u}^{\text{after}}(t)$ be the parameters after; then our assumption of a forward transit implies that $\mathbf{u}^{\text{after}}(t) = -\mathbf{u}^{\text{before}}(t)$, and this together with $\mathbf{r}^{\text{before}}(t) = \mathbf{r}^{\text{after}}(t)$ implies

$$\mathbf{R}^{\text{after}} = \mathbf{R}^{\text{before}} + 2\mathbf{u}^{\text{before}}(t). \quad (54)$$

This is the change in \mathbf{R} produced by a transit. We choose to leave the unit vectors $\hat{\mathbf{w}}_\lambda$ in Equation (53) unaffected by transits, leaving only the effect on the phases α_λ to be determined. They must change in such a way as to reverse the sign of $\mathbf{u}(t)$ but conserve $\mathbf{v}(t)$; since $\mathbf{u}(t)$ is a sum of sines while $\mathbf{v}(t)$ is a sum of cosines, this is easily done by reversing the signs of the arguments $(\omega_\lambda t + \alpha_\lambda)$ in Equation (51). Let the transit occur at time t_0 ; then $\omega_\lambda t_0 + \alpha_\lambda^{\text{after}} = -(\omega_\lambda t_0 + \alpha_\lambda^{\text{before}})$ so

$$\alpha_\lambda^{\text{after}} = -2\omega_\lambda t_0 - \alpha_\lambda^{\text{before}}. \quad (55)$$

Thus, a transit is implemented at time t_0 by leaving the $\hat{\mathbf{w}}_\lambda$ alone and making the substitutions

$$\begin{aligned} \mathbf{R} &\rightarrow \mathbf{R} + 2\mathbf{u}(t_0) \\ \alpha_\lambda &\rightarrow -2\omega_\lambda t_0 - \alpha_\lambda. \end{aligned} \quad (56)$$

This conserves $\mathbf{r}(t)$, reverses the sign of $\mathbf{u}(t)$, and conserves $\mathbf{v}(t)$.

Let the temperature-dependent rate at which transits occur be denoted ν , so in small time interval Δt a transit occurs with probability $\nu\Delta t$. As a transition rate, ν would ideally be calculated from matrix elements of the term in the Hamiltonian responsible for transits using Fermi's Golden Rule, and we will revisit this possibility in Section 6, but for now we will take the simpler path of fitting ν to the results of MD simulations.

Now the model consists of two parts. (a) Between transits, the average particle oscillates as given by Equations (51) and (53), with the phases α_λ and unit vectors $\hat{\mathbf{w}}_\lambda$ assigned randomly. (b) In each small time interval Δt a transit occurs with probability $\nu\Delta t$; if it occurs, it replaces \mathbf{R} and the α_λ with new values according to Equation (56). With the addition of transits, we can no longer express $\mathbf{r}(t)$ and $\mathbf{v}(t)$ in closed form at all times, so we no longer have a closed form for $Z(t)$; but the model can be implemented easily

on a computer, and then the data from the run can be used to calculate $Z(t)$ and $\hat{Z}(t)$ in a manner analogous to an MD simulation.

In [23] we calculated $\hat{Z}(t)$ in this fashion and compared the results with MD simulations of sodium with $N = 500$ and $\delta t = 0.2t^*$. We performed equilibrium runs of the system at temperatures ranging from the glassy regime to nearly three times the melting temperature of 371 K. At the two lowest temperatures for which we ran MD, the system remained in a single potential valley, as could be seen from examining the mean-squared displacement; so these runs were compared to the model using $\nu = 0$. For each of the higher temperatures, we ran the model for various values of ν , adjusting until the model matched the value of the first minimum of $\hat{Z}(t)$. Figures 12 through 15 compare the model's predictions with a representative sample of our MD results; the full set of results may be found in [23]. In all figures, the transit rate is expressed as a multiple of τ^{-1} , where τ , the mean vibrational period in a random valley, is given in Subsection 3.1. Note that all transit rates are on the order of τ^{-1} , supporting the contention made above that transits occur roughly once per mean vibrational period.

The most obvious trend in $\hat{Z}(t)$ is that its first minimum is rising with increasing T ; this is the primary reason for the increasing diffusion coefficient D . Note that the model is able to reproduce this most important feature quite satisfactorily. In fact, all fits of the model to the MD results capture their essential features, but we do see systematic trends in the discrepancies. First, note that the location of the first minimum barely changes at all in the model as ν is raised, but in MD the first minimum moves steadily to earlier times as the temperature rises. The first minimum occurs at a time roughly equal to half of the mean vibrational period, so the steady drift backward suggests that the MD system is sampling a higher range of frequencies at higher T . Also, in Figures 13 and 14 the model tends to overshoot the MD result in the vicinity of the first two maxima after the origin, and in Figure 15 this overshoot is accompanied by a positive tail that is slightly higher than the (still somewhat long) tail predicted by MD. These overshoots should clearly affect the diffusion coefficient D . To check this, we calculated the reduced diffusion coefficient \hat{D} , the integral of $\hat{Z}(t)$, which is related to D by $D = (k_B T / M) \hat{D}$. The results are compared to the values of \hat{D} calculated from the MD runs in Figure 16. This figure includes all of the data from [23], including the data not reproduced here. In all of the transiting cases, the model overestimates \hat{D} by roughly the same amount, which we take to be the effect of the overshoots at the first two maxima. At the higher temperatures

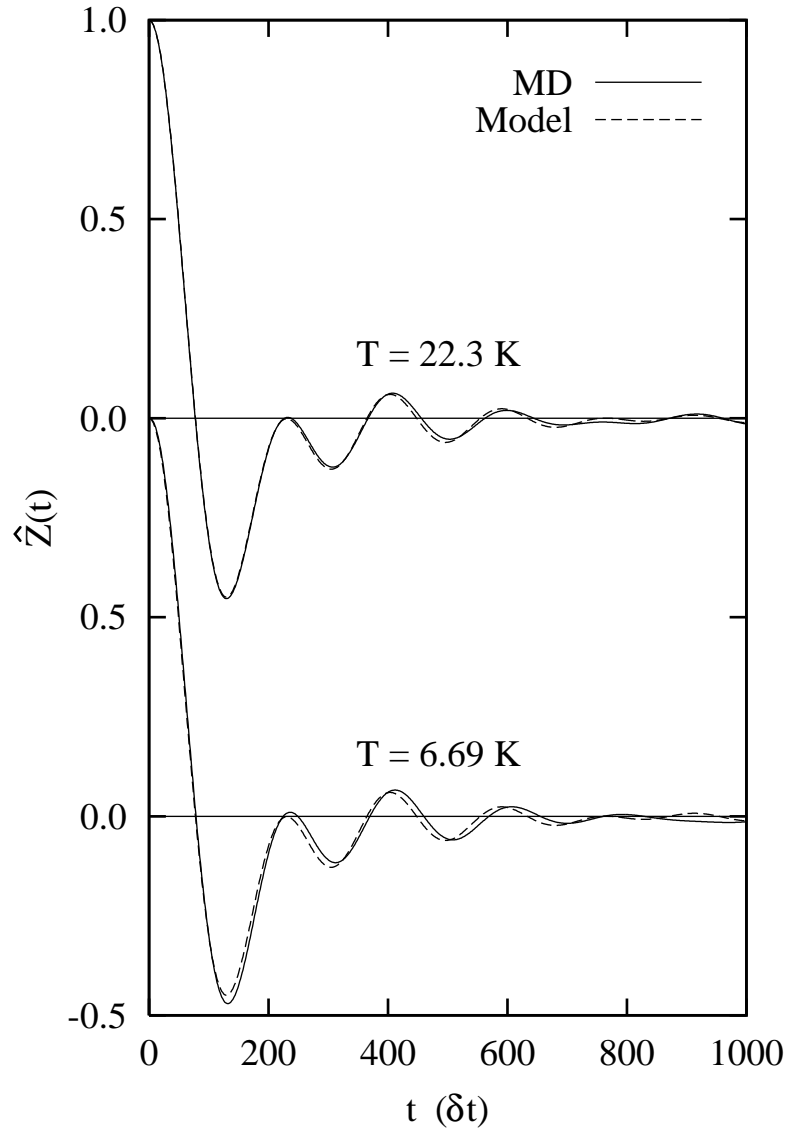


Figure 12: The model prediction for $\hat{Z}(t)$ at $\nu = 0$ compared with MD results for glassy liquid Na at $T = 6.69$ K and $T = 22.3$ K. From [23].

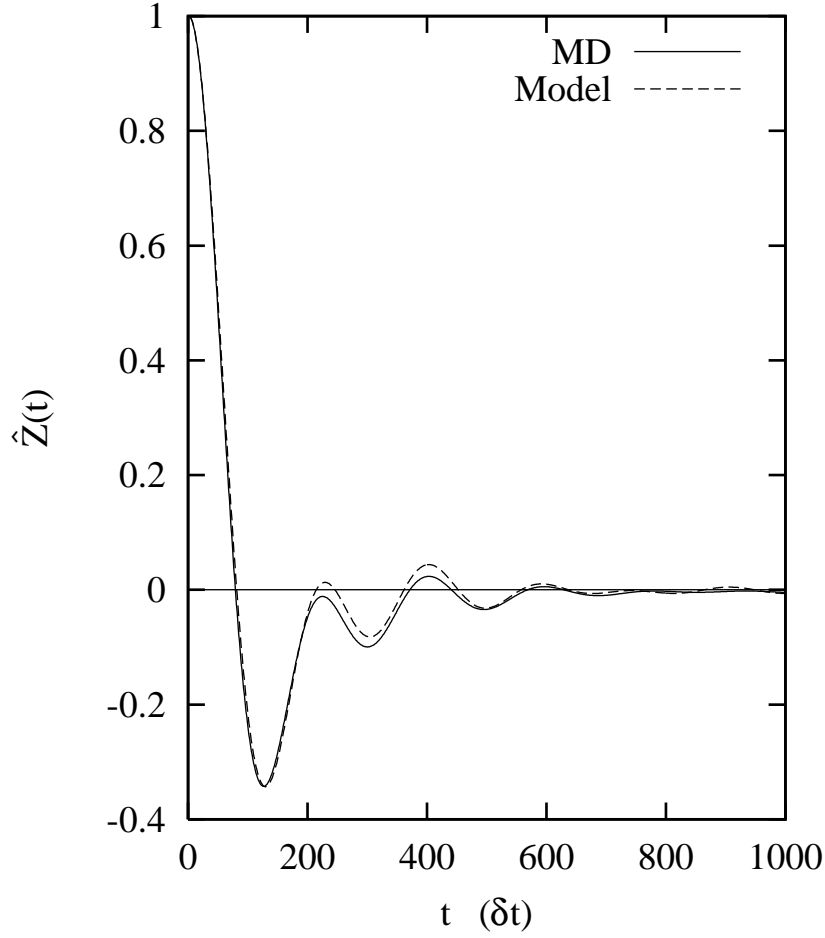


Figure 13: The model prediction for $\hat{Z}(t)$ at $\nu = 0.35018 \tau^{-1}$ compared with the MD result for supercooled liquid Na at $T = 216.3$ K. From [23].

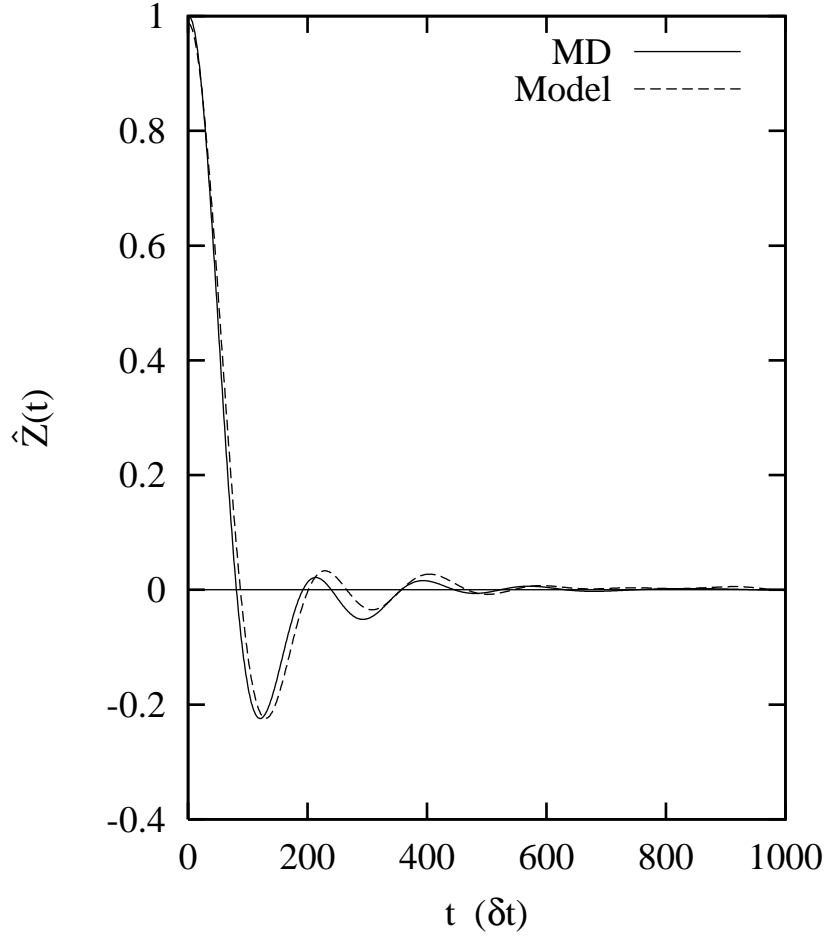


Figure 14: The model prediction for $\hat{Z}(t)$ at $\nu = 0.83985 \tau^{-1}$ compared with the MD result for liquid Na at $T = 425.0$ K. From [23].

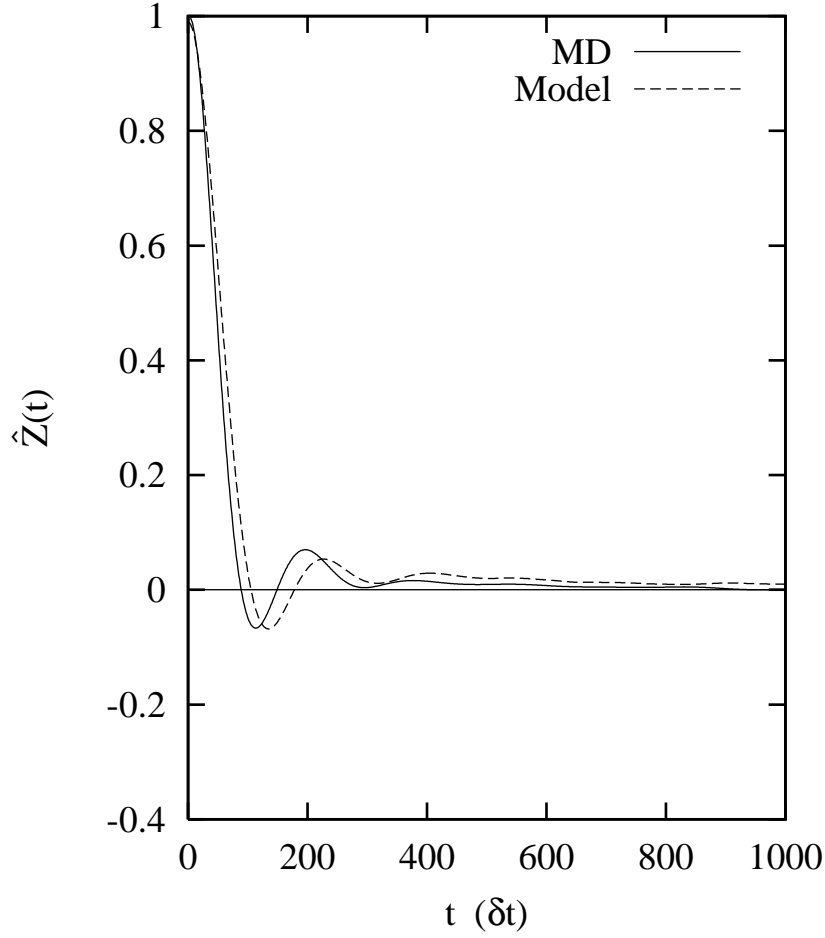


Figure 15: The model prediction for $\hat{Z}(t)$ at $\nu = 1.68774 \tau^{-1}$ compared with the MD result for liquid Na at $T = 1022.0$ K. From [23].

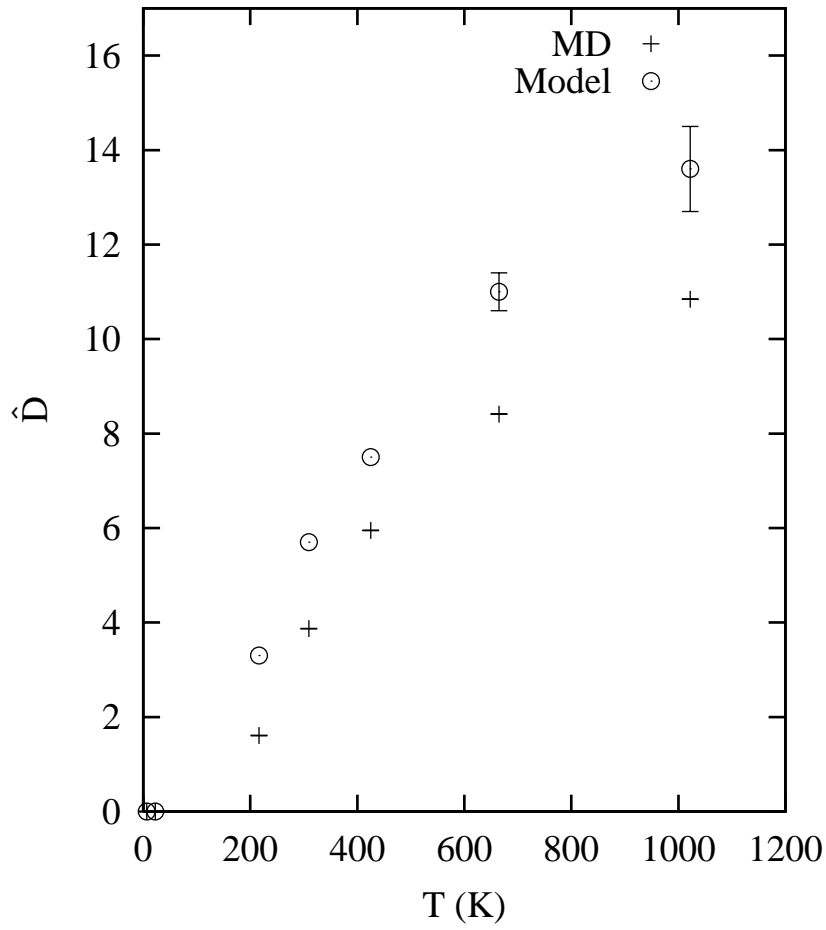


Figure 16: \hat{D} as a function of T for both the model and MD. From [23].

the discrepancy is also slightly higher, presumably due to the model's long tail.

Although this single-particle model is promising, it is clearly based on some arbitrary choices; possible improvements, taking advantage of the information about transits from Subsection 3.1, will be discussed briefly in the next section.

6 Outlook

6.1 What we've learned

Two sets of experimental data on monatomic liquids, their specific heats at the melting point and entropy of melting, led to two hypotheses concerning their behavior:

1. The many-body potential surface of a monatomic liquid is composed of approximately w^N intersecting nearly-harmonic valleys which fall into three classes: crystalline, symmetric, and random. The random class dominates the potential surface, and in the large- N limit these valleys all have the same depth, vibrational spectrum, and radial and angular distribution functions at the valley minimum.
2. The motion of the system decomposes into two types: Oscillation in a single many-body valley, and transits, which are nearly-instantaneous transitions between valleys.

The picture that arises from these hypotheses has been tested successfully with computer simulations of sodium and Lennard-Jones argon, and it has been used to develop accounts of equilibrium and nonequilibrium statistical mechanics of monatomic liquids which compare very favorably with experiments and simulations. Both of these insights have demonstrated their value, and they should be taken into account in any attempt at a comprehensive theory of monatomic liquids.

6.2 Further developments

Work in any of the following areas would be of great interest.

6.2.1 Studies of the potential energy landscape

The crystalline valleys have been studied for decades and are by now well understood. Anharmonic effects in these valleys are complicated but small in magnitude. We need to know more, however, about the random valleys, because of the dominant role they play in equilibrium statistical mechanics. The particle configurations of the random valley structures in sodium, for example, need to be characterized more completely than simply determining $G_\gamma(r)$. Do they lack any remnants of crystal symmetry, as asserted? It would also be worthwhile to continue the studies of argon above its critical density (and other noble gas liquids) until its properties are as well characterized as sodium's are. The remaining nearly-free-electron metals (22 or so elements) are expected to behave as sodium does, considering the results of pseudopotential theory for these metals; but that should be verified. Finally, most of the remaining elements in the periodic table that form monatomic liquids are non-nearly-free-electron metals (such as the transition metals), and electronic structure theory is just now reaching the point that their interatomic potentials can be calculated reliably. Whether they also admit a division of their many-body potential valleys into similar classes would be interesting to discover.

The symmetric valleys are the least studied in any of the elements we have considered, and they will be important if we wish to understand a real monatomic liquid that happens to quench into such a valley. (An experimental example of such a case is the amorphous carbon structure in [31], cited in Subsection 2.2.) The distributions of Φ_0 values and normal mode spectra $g(\omega)$, among other quantities, should be determined.

Finally, we have asserted that the number of valleys is universally w^N , where $\ln w = 0.8$, and that the randoms so outnumber the others that virtually all the valleys are random. Is this so? Can the valleys be counted? It would be of tremendous interest to see if the number of valleys approximately obeys this relation, since it is crucial to much of the theory.

6.2.2 Properties of anomalous melters

Although the anomalous melters undergo substantial changes in their electronic structure upon melting, they should obey the same liquid dynamics theory as the normal melters; how they become liquids should not affect how they behave once they are liquids. However, as we saw in Subsection 4.4,

the values of Θ_0 and S_E for these elements should differ greatly between the liquid and crystal, and these differences should account for the bulk of their entropy of melting; testing this would be a very strong check on the theory of liquids we have proposed.

6.2.3 Extensions of equilibrium theory

We have noted that all equilibrium thermodynamic quantities have both anharmonic and boundary corrections, and theories of both of these need to be developed. Consider as an example C_I , the ionic part of the specific heat, which the theory predicts to be $C_I = 3Nk_B + C_{AB}$ (cf. Equation (33)). At the melting point, C_I for the liquid, as for the crystal, shows small anharmonic effects, and these appear to be of roughly the same sign and magnitude for both phases (see Figure 1). Typically the full C_V decreases as T increases, with C_I ultimately falling to the value for the gas, $(3/2)Nk_B$, and given the above comments on the anharmonic effects, we expect the boundary correction to be mostly responsible for this decrease. One's classical intuition suggests that the boundary correction is in fact negative, and this intuition is confirmed by calculations of the correction resulting from cutting off the potential of a one-dimensional harmonic valley [17]. Further work on these corrections, however, remains to be done.

Another significant anharmonic effect which is not yet understood is the fact that the equilibrium states occupying the random valleys in Figure 5 and Figure 4 of [19] do not follow a straight line of unit slope at higher temperatures; this is why the change in Φ_0 between crystal and liquid is not closer to $T_m\Delta S$, as discussed in Subsection 4.4. Is this feature associated with the onset of diffusion? Is it present in other elements, or is it unique to sodium? This effect is quite significant and demands further study.

6.2.4 Extensions of nonequilibrium theory

We have discussed only one correlation function of interest, $Z(t)$, and it remains to apply the picture to several others, such as the stress-stress autocorrelation functions, which determine the shear and bulk viscosities, and the dynamic structure factor $S(\mathbf{q}, \omega)$, which determines the liquid's neutron scattering cross section in the Born approximation. Another area of interest is the glass transition. It has been shown that thermal properties of a material during the glass transition depend on the cooling rate [42, 43, 44] and that

if cooling or heating stops while the system is undergoing the transition, it will then relax to an equilibrium state [43, 45]. This indicates that the glass transition involves significant nonequilibrium behavior. A first attempt at a description of the glass transition using transits may be found in [22], and further development of that line of work is needed.

Several questions involving the picture’s conception of transits also need to be addressed. First, does the picture accurately portray the mechanism by which liquids diffuse at higher temperatures? We have seen that in low-temperature simulations transits occur in precisely the manner predicted (Subsection 3.1), but that does not rule out the possibility of a qualitative change in behavior as temperature increases. What is the role of precursors and postcursors, which currently are not incorporated into the picture? Perhaps they indicate that the instantaneous transit is only a first approximation, to be replaced by a more detailed process that unfolds over a very small but finite time. If the picture of transits needs to be revised, then the revisions should affect the nonequilibrium theory noticeably. Then there is the specific transit model used in our calculations of $Z(t)$: It accounts for the upward shift in the first minimum in $Z(t)$, but it requires the transit amplitude to vary as $T^{1/2}$ (because it equates the size of a transit to the amplitude of oscillation of a typical particle), and a softer T dependence is likely more accurate. Also, the transit amplitudes it predicts at the temperatures of the simulations in Subsection 3.1 are smaller than the observed amplitudes by roughly a factor of two. Then, as we have already noted, in principle one should be able to compute the transit rate ν using the Golden Rule and the matrix element of the transition term in the Hamiltonian between two states isolated in distinct valleys. This would be a very challenging calculation, but it would give us tremendous insight into the mechanics of the transit process. Note also that ν and the boundary corrections X_B to the thermodynamic quantities ultimately arise from the same source: the boundary term in the Hamiltonian. As such, the two should be related, and a theory of that relationship remains to be developed.

6.3 The role of this theory

This theory of monatomic liquid dynamics is based on a Hamiltonian, from which both equilibrium and nonequilibrium properties follow, in either quantum or classical regimes, according to the well-developed principles of many-body physics. The nearly harmonic character and the statistical domi-

nance of the random potential valleys render equilibrium statistical mechanics tractable to leading order, and they lead to well-defined corrections beyond leading order. Decomposition of the motion into intra-valley oscillations and inter-valley transits provides a basis from which time-correlation functions can in principle be calculated from their definitions in terms of the mechanical motion of the system. In comparison, to our knowledge QNM and INM theories have been developed only for the calculation of correlation functions. Both work with an averaged normal mode frequency distribution $\langle g(\omega) \rangle$: QNM theories average over configurations at the bottoms of potential valleys, while INM theories compute a temperature-dependent average over the entire configuration space. Although neither of these quantities enters the system's Hamiltonian, we can see that the QNM $\langle g(\omega) \rangle$ can in principle approximate $g(\omega)$ for a single random valley. When all is said and done, however, the ultimate theoretical approach to this or any other problem is through its Hamiltonian. We believe that the ideas presented here provide a useful framework for thinking about monatomic liquid dynamics, whether one is refining equilibrium calculations to achieve improved agreement with experiment or designing and analyzing experiments to learn more about nonequilibrium processes.

Acknowledgments

The authors gratefully acknowledge Brad Clements for his support and collaborations. This work was supported by the U. S. DOE through contract W-7405-ENG-36.

References

- [1] J. Frenkel, Z. Phys. **35**, 652 (1926).
- [2] J. Frenkel, *Kinetic Theory of Liquids* (Clarendon, Oxford, 1946), Chap. III, Sec. 1.
- [3] F. H. Stillinger and T. A. Weber, Phys. Rev. A **25**, 978 (1982).
- [4] T. A. Weber and F. H. Stillinger, J. Chem. Phys. **80**, 2742 (1984).
- [5] F. H. Stillinger, Science **267**, 1935 (1995).

- [6] E. Rabani, J. D. Gezelter, and B. J. Berne, J. Chem. Phys. **107**, 6867 (1997).
- [7] A. Pohorille, L. R. Pratt, R. A. LaViolette, M. A. Wilson, and R. D. McElroy, J. Chem. Phys. **87**, 6070 (1987).
- [8] E. Rabani, J. D. Gezelter, and B. J. Berne, J. Chem. Phys. **110**, 3444 (1999).
- [9] G. Seeley and T. Keyes, J. Chem. Phys. **91**, 5581 (1989).
- [10] T. Keyes, J. Phys. Chem. A **101**, 2921 (1997).
- [11] B.-C. Xu and R. M. Stratt, J. Chem. Phys. **91**, 5613 (1989).
- [12] M. Buchner, B. M. Ladanyi, and R. M. Stratt, J. Chem. Phys. **97**, 8522 (1992).
- [13] E. F. David and R. M. Stratt, J. Chem. Phys. **109**, 1375 (1998).
- [14] S. D. Bembenek and B. B. Laird, J. Chem. Phys. **104**, 5199 (1995).
- [15] T.-M. Wu, W.-J. Ma, and S. L. Chang, J. Chem. Phys. **113**, 274 (2000).
- [16] D. C. Wallace, Phys. Rev. E **56**, 4179 (1997).
- [17] D. C. Wallace, Phys. Rev. E **57**, 1717 (1998).
- [18] D. C. Wallace, Phys. Rev. E **58**, 538 (1998).
- [19] D. C. Wallace and B. E. Clements, Phys. Rev. E **59**, 2942 (1999).
- [20] B. E. Clements and D. C. Wallace, Phys. Rev. E **59**, 2955 (1999).
- [21] E. D. Chisolm, B. E. Clements, and D. C. Wallace, unpublished.
- [22] D. C. Wallace, Phys. Rev. E **60**, 7049 (1999).
- [23] E. D. Chisolm, B. E. Clements, and D. C. Wallace, Phys. Rev. E **63**, 031204 (2001); **64**, 019902 (2001).
- [24] D. C. Wallace, E. D. Chisolm, and B. E. Clements, Phys. Rev. E **64**, 011205 (2001).

- [25] R. Hultgren, P. D. Desai, D. T. Hawkins, M. Gleiser, K. K. Kelley, and D. D. Wagman, *Selected Values of the Thermodynamic Properties of the Elements* (American Society for Metals, Metals Park, Ohio, 1973).
- [26] M. W. Chase, Jr., C. A. Davies, J. R. Downey, Jr., D. J. Frurip, R. A. McDonald, and A. N. Suyverud, J. Phys. Chem. Ref. Data **14**, Suppl. 1 (1985).
- [27] V. L. Moruzzi, J. F. Janak, and A. R. Williams, *Calculated Electronic Properties of Metals* (Pergamon, New York, 1978).
- [28] D. A. Papaconstantopoulos, *Handbook of the Band Structure of Elemental Solids* (Plenum, New York, 1986).
- [29] D. C. Wallace, Proc. R. Soc. Lond. A **433**, 631.
- [30] D. C. Wallace, Phys. Rev. E **56**, 1981 (1997).
- [31] D. R. McKenzie, D. Muller, and B. A. Pailthorpe, Phys. Rev. Lett. **67**, 773 (1991).
- [32] W. A. Harrison, *Pseudopotentials in the Theory of Metals* (Benjamin, New York, 1972).
- [33] D. C. Wallace, *Thermodynamics of Crystals* (Dover, New York, 1998).
- [34] D. C. Wallace, Phys. Rev. **176**, 832 (1968).
- [35] M. P. Allen and D. J. Tildesley, *Computer Simulations of Liquids* (Oxford University Press, Oxford, 1990).
- [36] L. B. Davies and P. J. Grundy, Phys. Status Solidi A **8**, 189 (1971).
- [37] T. Ichikawa, Phys. Status Solidi A **19**, 707 (1973).
- [38] M. R. Bennett and J. G. Wright, Phys. Status Solidi A **13**, 135 (1972).
- [39] P. K. Leung and J. G. Wright, Philos. Mag. **30**, 995 (1974).
- [40] J. P. Hansen and I. R. McDonald, *Theory of Simple Liquids* (Academic, London, 1986).
- [41] R. Zwanzig, J. Chem. Phys. **79**, 4507 (1983).

- [42] M. D. Ediger, C. A. Angell, and S. R. Nagel, J. Phys. Chem. **100**, 13200 (1996).
- [43] C. A. Angell, J. H. R. Clarke, and L. V. Woodcock, in *Advances in Chemical Physics*, edited by I. Prigogine and S. A. Rice (Wiley Interscience, New York, 1981), Vol. 48, p. 397.
- [44] K. Vollmayr, W. Kob, and K. Binder, J. Chem. Phys. **105**, 4714 (1996).
- [45] C. A. Angell, J. Non-Cryst. Solids **102**, 205 (1988).